DIPLOMA THESIS

Bio-sensor embedding for biofeedback based closed-loop auricular Vagus Nerve Stimulation

carried out for the purpose of obtaining the degree of

Dipl.-Ing.

in

Biomedical Engineering

by

Lukas Santner, BSc

51831924

under the supervision of

Univ.Ass. Dipl.-Ing. Babak Dabiri Razlighi

Univ.Prof.Dipl.-Ing. Dr.techn. Eugenijus Kaniusas

Institute of Biomedical Electronics

Vienna, September 2022

Eidesstattliche Erklärung

Ich erkläre an Eides statt, dass ich die vorliegende Diplomarbeit selbstständig und ohne fremde Hilfe verfasst, andere als die angegebenen Quellen und Hilfsmittel nicht benutzt bzw. die wörtlich oder sinngemäß entnommenen Stellen als solche kenntlich gemacht habe.

Datum	Lukas Santner

Kurzfassung

Die aurikuläre Vagusnervstimulation (aVNS) ist eine Behandlungsmethode für chronische Krankheiten wie Epilepsie und Depression. Sie wird hauptsächlich als Open-Loop-System ohne direktes Feedback durchgeführt. Die Behandlung erhält also keine Informationen über den physiologischen Zustand des Patienten. Ein Closed-Loop Konzept hingegen erhält Rückmeldungen und kann Vorgänge wie eine Unter- oder Überstimulation korrigieren. Um dies zu ermöglichen, müssen die Patientenparameter als Echtzeit-Biofeedback aufgenommen und analysiert werden.

Eine bereits etablierte aVNS Closed-Loop Anwendung an der TU Wien wird in dieser Arbeit verwendet. Sie erfasst den Herzzyklus des Patienten und stimuliert den nachfolgenden Zyklus in einer ausgewählten Phase. Für diese Diplomarbeit wird das BIOPAC System durch den MAX86150 Sensor von Maxim Integrated ersetzt um portables Biofeedback anhand von Elektrokardiographie und Photoplethysmographie zu liefern. Der Sensor wurde mit einer Samplingfrequenz von 800Hz eingerichtet und überträgt alle 25ms Daten. Für die Implementierung wurden neue Filter erstellt, die Kalibrierung angepasst und die Latenzzeit des Systems bestimmt. Nach kompensierter Latenz wurden die beiden Versuchsaufbauten hinsichtlich ihrer Leistung verglichen.

Die Latenzzeit des entwickelten Aufbaus wurde mit 96 $\pm$27.1ms (Mittelwert $\pm$Standard abweichung) festgestellt und kompensiert. Das MAX-Setup stimulierte mit einem std von $\pm$67.2ms um den gewünschten Zielpunkt, während die BIOPAC-Anwendung einen std von $\pm$67.1ms ergab. Bei der durchgeführten Messung erfasste der MAX-Sensor etwa 19% mehr Herzzyklen als das BIOPAC-System. Die Stimulationsgenauigkeit des MAX-Setups beträgt $\pm$13.3ms.

Die Latenzzeit des MAX-Setups steigt auf 96ms im Vergleich zum TU Wien Setup mit 85ms. Beide Versuchsaufbauten schneiden bei der gezielten Stimulationsauslösung in Abhängigkeit des Herzzyklus gleich gut ab. Die Präzision ist auf einen std von $\pm$13.3ms beschränkt, da die Messdaten alle 25ms übertragen werden.Um diese Präzision zu erreichen, ist ein besserer Vorhersagealgorithmus erforderlich, um den herzfrequenzvariabilitätsabhängigen Zielpunkt im Herzzyklus genau vorherzusagen und stimulieren zu können.

Der neu implementierte Sensor MAX86150 ist ein guter Ersatz für das BIOPAC-System. Durch das Ersetzen wird die letzte stationäre Komponente entfernt. Damit bietet der Versuchsaufbau eine Grundlage für die weitere Entwicklung eines tragbaren aVNS-Systems mit geschlossenem Regelkreis.

Abstract

Auricular vagus nerve stimulation (aVNS) is a treatment method for chronic diseases such as epilepsy and depression. It is mainly carried out as an open-loop system without direct feedback. Thus, the treatment does not receive information about the patient's physiological conditions. A closed-loop approach receives feedback and can correct the stimulation, like under or overstimulation. To make this possible, patient parameters must be recorded and analysed in real-time.

An already established aVNS closed-loop application at the TU Wien is utilized in this work. It detects the patient's cardiac cycle and stimulates the subsequent cycle in a selected phase. For this thesis, the MAX86150 sensor from Maxim Integrated, recording electrocardiography & photoplethysmography, replaces the BIOPAC System to provide portable biofeedback acquisition. The sensor was set up with a 800Hz sampling frequency and transfers data every 25ms. For the implementation, new filters were designed, the calibration was adapted and the latency of the system was determined. Both experimental setups were compared based on their performance.

The latency of the developed setup was determined to be 96 ±27.1ms (mean ±standard deviation) and compensated. The MAX setup stimulated with an std of ±67.2ms around the desired target point, while the BIOPAC application produced an std of ±67.1ms. For the performed measurement the MAX sensor detected approximately 19% more cardiac cycles than the BIOPAC system. The stimulation precision of the MAX setup is ±13.3ms.

The MAX setup latency increased to 96ms compared to the TU Wien setup with 85ms. Both experimental setups perform equally in target stimulation initiation based on cardiac events. However, the MAX setup has shown a higher rate in cardiac cycle detection. The setup precision is limited to an std of ±13.3ms due to the data transmission every 25ms. To achieve this precision, a better prediction algorithm is needed to accurately predict and stimulate the heart rate variability dependent target point in the cardiac cycle.

The newly implemented MAX86150 sensor is a good replacement for the BIOPAC system. With the replacement, the last stationary component is removed. Thus, the experimental setup provides a basis for the further development of a portable closed-loop aVNS system.

Acknowledgement

First of all, I would like to thank my supervisor, Univ.Ass. Dipl.-Ing. Babak Dabiri Razlighi for the excellent supervision of the master's thesis. I want to thank him for his guidance, support and constructive criticism throughout the whole process. Without him, this thesis would not have been possible.

I would like to express my gratitude to my dean and second supervisor Univ.Prof.Dipl.-Ing. Dr.techn. Eugenijus Kaniusas for his inspiring lectures and reliable support throughout my studies.

Finally, I would like to thank my family and friends for their everlasting encouragement and support.

Contents

Acronyms and Variables

ADC	Analog to Digital Converter
ANS	Autonomic Nervous System
AV node	Atrioventricular node
aVNS	Auricular Vagus Nerve Stimulation
BOSD	BIOPAC Operating Stimulation Design
bpm	Beats Per Minute
CRC	Cyclic Redundancy Check
DMA	Direct Memory Access
EBS	Embedded Biosensor System/Stimulation
ECG	Electrocardiogram
FES	Functional Electrical Stimulation
FIFO	First In First Out
FP	False Positive
HRV	Heart Rate Variability
LED	Light-Emitting Diode
MCU	Microcontroller Unit
PNS	Parasympathetic Nervous System
PPG	Photoplethysmogram
pVNS	Percutaneous Vagus Nerve Stimulation
SA node	Sinoatrial node
SCL	Serial Clock Line
SDL	Serial Data Line
SDNN	Standard Deviation between NN Intervals
SNS	Sympathetic Nervous System
TP	True Positive
tVNS	Transcutaneous Vagus Nerve Stimulation
UART	Universal Asynchronous Receiver-Transmitter
VNS	Vagus Nerve Stimulation

$t_{\text{Communication}}$	Time of Device Communication
$\triangle t_{\text{Delay}}$	Time Delay to the next Stimulation
$t_{\text{HardwareDelay}}$	Time of Hardware Delay
$t_{\text{Processing}}$	Time of Processing Tasks
t_{RQ}	Time of a RQ Interval
$t_{\text{Stimulation}}$	Time until Stimulation
$\hat{p}_{ij}$	Cross Correlation Coefficient
x_i & x_j	Elements of a Dataset
$\bar{x}_i$ & $\bar{x}_j$	Mean of a Dataset

1 Introduction

The health industry nowadays treats patients mainly with drugs, surgery, and therapy. However, besides these methods, there is another option, electrostimulation. Electrostimulation is the application of electric pulses to individuals at various locations to achieve a multitude of effects. Almost every function in the body can be traced back to the nervous system and therefore electric signals. Muscles are contracted by nerves. Nerves provide the central nervous system with information about the state of the body and can influence hormone release through the endocrine system. During exercise, the body's oxygen demand is increased. To accommodate, the supply is upped by expanding the lungs via the peripheral nervous system. The nerves have an influence everywhere. Thus, the nervous system is an ideal input for electrostimulation therapies [1].

One example is functional electrical stimulation (FES). Stroke victims lose their ability to move to a certain degree. Spinal cord injuries can be even more severe to the patients' freedom of movement. Here, FES can be an additional tool besides physiotherapy for recovery. It is a treatment for stimulating muscles to provide patients with support in their motor function. Short electrical impulses are applied to contract a variety of muscle groups, which together, for example, bend the knee. Such sequences can be used to mimic walking, cycling, and other movements. FES enables injured people to regain much of their freedom and can speed up their recuperation. [2].

The electrostimulation has generally been around for a long time as pacemakers and defibrillators. They use shocks/impulses to treat heart conditions. Another treatment utilizes deep brain stimulation for people with Parkinson's disease or depression [3].

Electrostimulation is also used in the Vagus Nerve Stimulation (VNS). The following chapters will introduce the Vagus Nerve and different approaches as well as treatments of VNS. Furthermore, the biosignal recording methods electrocardiography and photoplethysmography will be introduced. They are utilized in the closed loop VNS setup documented. Finally, the objective of this thesis will be stated.

1.1 Vagus Nerve

The Vagus Nerve is spread over a wide area of the body, collecting information and influencing various functions. A range of conditions can be treated through its stimulation. An emerging treatment technique is the auricular Vagus Nerve Stimulation (aVNS).

1.1.1 Anatomy and Physiology

The Vagus Nerve is the 10th nerve of the brain [4]. It is part of the Parasympathetic Nervous System (PNS) with an opposing force being the Sympathetic Nervous System (SNS), which in turn are a part of the Autonomic Nervous System (ANS). Typically, explanations call the PNS the "rest and digest" and the SNS the "fight or flight" system [5]. For this work, the Vagus Nerve and therefore also the PNS are of main interest. Figure 1.1 provides an overview of organs that the Vagus Nerve is involved in. It extends its branches, among others, to the auricle, pharynx, larynx, and esophagus. Then wandering further down into the thorax and abdomen, covering the stomach, intestines, lung, heart, etc [6].

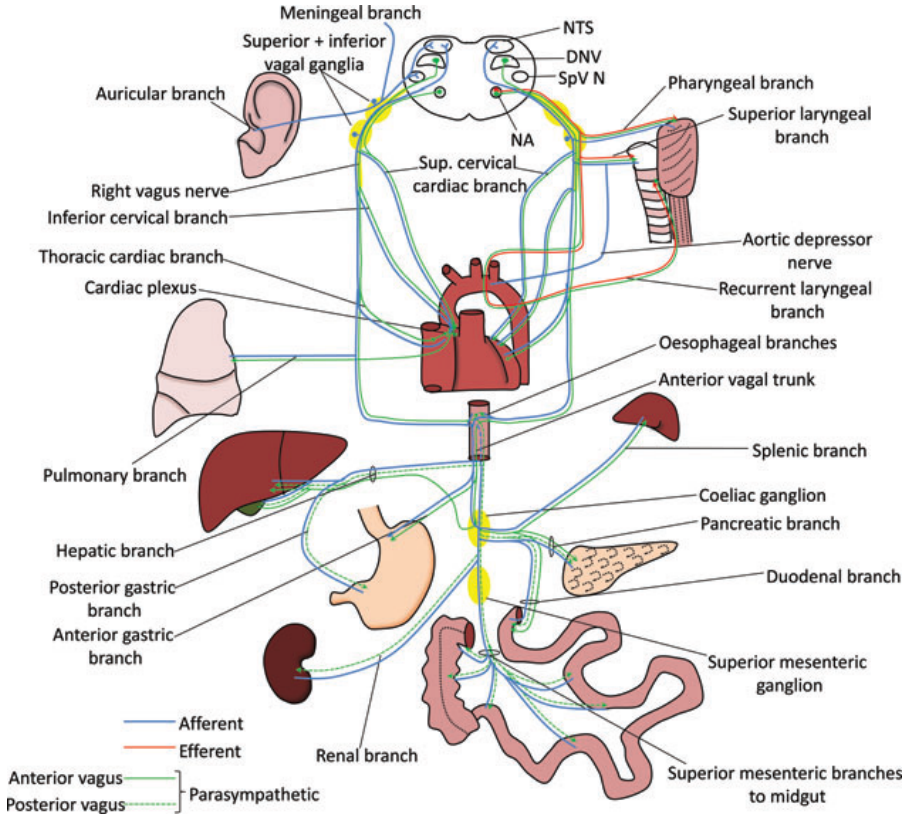

Figure 1.1: Illustration of Vagus Nerve connection to structures of the body [7].

It should be noted that only 20% of the branches are of efferent type [7]. They influence the increase of peristalsis, reduction of heart rate, secretion in the gastrointestinal tract,

and bronchoconstriction (respiratory rate) [4]. The other 80% represent afferent pathways, providing sensory feedback of various organs [7]. Therefore, its most important task is to provide the brain with information regarding the state of the body [8].

1.1.2 Vagus Nerve Stimulation

Preclinical studies in animals with seizures approximately 30 years ago incentivized investigations into the effects of VNS as a treatment method. One such study in 1994, with a randomized, parallel, double-blind setup, studied the effect of VNS implants on patients over a 14-week timeframe. All participants had refractory partial seizures and were given either an implant with high or low VNS. The group with high VNS had a mean reduction of 30.9% in seizure frequency compared to 11.3% in low VNS patients [9]. Studies like this one led way to the first approvals of VNS for clinical application by the FDA in 1997 [10] and a Conformité Européenne marking in 1994 [11].

The target of these stimulations are the afferent pathways of the Vagus Nerve. An example would be the baroreflex, it is one of the feedback systems in charge of regulating blood pressure [12]. When the baroreceptors detect increased blood pressure, they transmit an afferent signal to the brain. This in turn triggers a sympathetic inhibition and parasympathetic heightening to decrease the heartbeat frequency [13]. The current VNS does not target a specific organ of the body. Instead, it influences the system as a whole, leading to general systemic effects like the sympatho-inhibition [12].

Unwanted side effects can occur during the stimulation of the patient. They mainly arise during active stimulation. These side effects include an altered voice, coughing, hoarseness, neck or throat pain, dyspnea, and others. According to Ben-Menachem of these side effects, "97.8% were reported as mild to moderate and usually resolved with a reduction in stimulation parameters" [14]. Another study suggests specifically a pulse width reduction with the added benefit of reducing battery consumption [15].

State of the art

The current state of the art for epilepsy is to implant a stimulation device under the clavicle on the left side, as seen in Figure 1.2. It is connected through a lead to the neck area of the patient. There, a helical electrode is wrapped around the left cervical vagus nerve for stimulation application. By applying current seizures can be prevented or treated acutely. The following different modes of operation exist [16].

- **Open-loop** approach applying continual current.
- **Closed-loop** setup taking the heart rate into account. Should the frequency exceed a certain threshold over the baseline, a stimulation cycle will be triggered.
- **On-demand** initiation in case the patient perceives an onset.

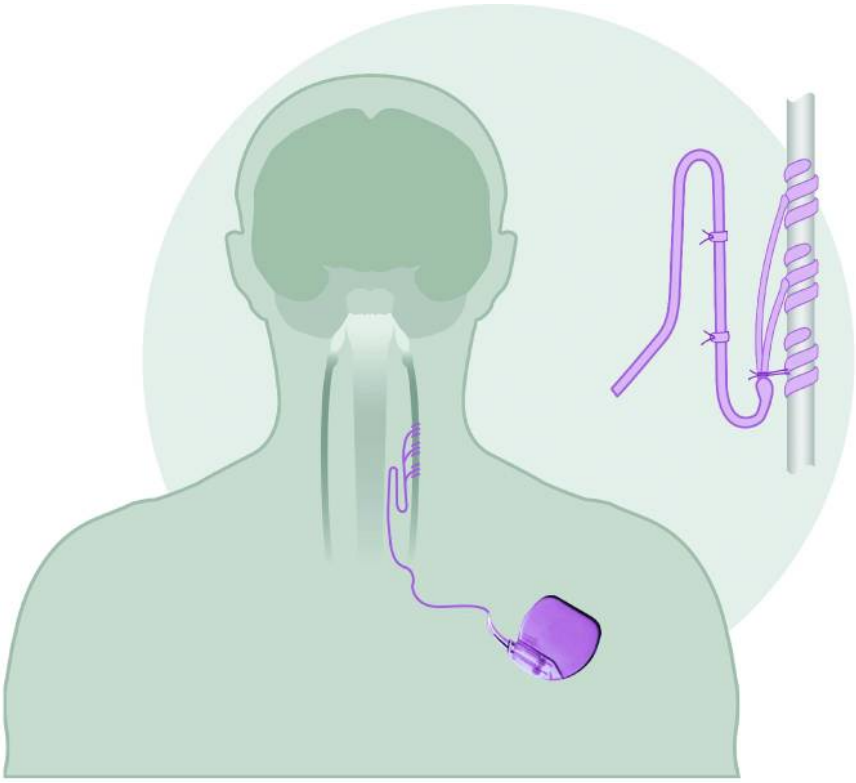

Figure 1.2: Vagus Nerve Stimulator implanted in the thorax with an electrode fixated to the Vagus Nerve in the neck region [17].

Apart from refractory epilepsy, VNS is also clinically utilized for depression [18], [19]. Furthermore, a lot of additional pre-clinical studies concerning other treatment possibilities of VNS exist.

- **Inflammatory Inhibition**
  Proinflammatory cytokine synthesis can be inhibited [20].
- **Psychiatric Disorders**
  Besides depression, studies show that VNS may also have an effect on other psychiatric disorders, but more research is needed. [21].
- **Pain**
  One study covered the treatment of chronic pelvic pain [22], another investigated the effect on headaches [23].
- **Atrial Fibrillation**
  A study and its follow up cover the treatment of paroxysmal atrial fibrillation and it's potential [24], [25].

1.1.3 Auricular Vagus Nerve Stimulation

The classical approach of stimulation carries some complications due to the necessary operation for implantation. Although it is minimally invasive, the surgery still bears some risk to the patient due to the delicate area operated on [26]. A new alternative method for VNS is in the process of emerging, the aVNS. It utilizes the Vagus Nerve branch extending to the ear region as seen in Figure 1.3a, circumventing the need for an implantation [12].

Depending on the region of the ear (Antihelix, Cavum conchae, Cymba conchae, and Tragus) different percentages of the situated nerves innervate the Vagus Nerve. The highest percentage is in the Cymba conchae, then Antihelix and Tragus & Cavum conchae equally [27]. Therefore, as shown in Figure 1.3b, the electrodes are typically placed at these locations. A study by Frangos et al. investigated via fMRI scans whether aVNS activates the Vagus Nerve as reliable as the classical approach. Their findings provide evidence of "significant activation of the "classical" central vagal projections" [28].

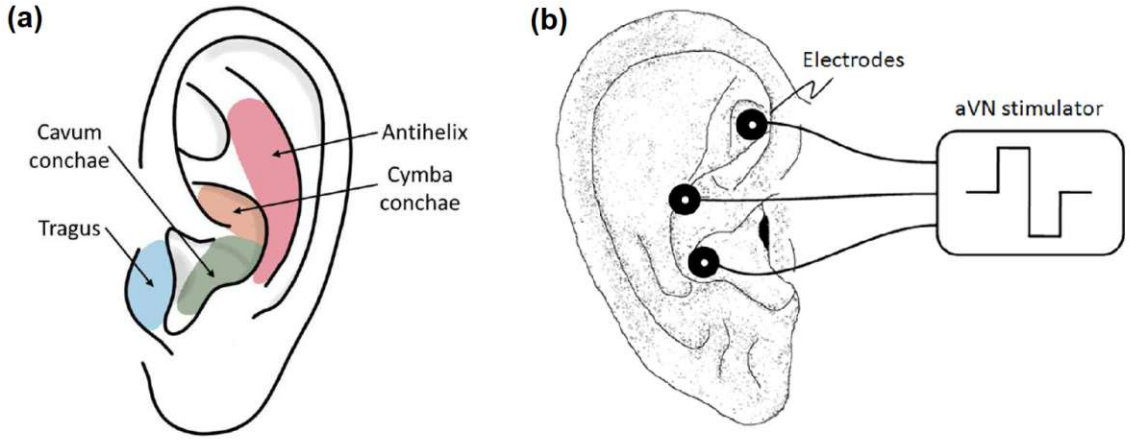

Figure 1.3: **(a)** Highlighted auricular areas correlating to the Vagus Nerve [26].
(b) Placement of electrodes for Auricular Vagus Nerve Stimulation [12].

In contrast to VNS, aVNS is a non-invasive treatment utilizing surface electrodes to stimulate. There are two options to innervate the nerves, by either percutaneous or transcutaneous aVNS.

- **Percutaneous VNS**
  The percutaneous approach applies needle electrodes to punctuate the skin and access inner body structures for stimulation. It is also sometimes called pVNS in literature.

- **Transcutaneous VNS**
  As opposed to pVNS, transcutaneous stimulation applies surface electrodes to affect inner structures by penetrating through the skin. It is referred to as tVNS.

Both approaches have their pro and contra. The pVNS is capable of innervating specific sites easily. The impedance is lower without a skin barrier, requiring less energy for stimulation. On the other hand, the insertion of needles in the skin leads to irritations and possible bleeding. Correct placement via established procedures can keep it to a minimum. The stimulation through the skin barrier when using tVNS avoids the insertion of needles, but affects a more widespread area, possibly influencing unwanted structures. Additionally, it requires a higher energy expenditure because of the increased impedance, which could reduce battery life (if present) [29].

1.2 Biosignals

The functions of the human body are controlled through biosignals of various nature. These signals can be extracted and interpreted to gain insight into the underlying biological system. There are different approaches to extract biosignals. The electric activity of the heart can be recorded with an Electrocardiogram (ECG) [30]. The blood flow created by the heart cycle on the other hand can be investigated with Photoplethysmogram (PPG) [31].

1.2.1 Electrocardiography

The contraction of the heart is a complex mechanism that maintains the blood flow of the body. Through it, blood can oxygenate the body, provide nourishment and remove waste material, etc. To fulfill this task the heart consists of electrically excitable muscle cells as well as a conduction system enabling an impulse to travel and innervate [32].

This conduction system starts with the Sinoatrial (SA) node advancing into the Atrioventricular (AV) node, His bundles, and finally Purkinje fibers as seen in Figure 1.4. The SA node is the natural pacemaker of the heart producing impulses at a certain frequency. Depending on the ANS, it generates them faster or slower. Its approximate maximum lies at 220 beats per minute (bpm) for young individuals. This impulse then travels along the aforementioned path and contracts the muscle cells in the process. First, the Atrium of the heart contracts, pumping blood into the Ventricles. Then, after a short delay at the AV node, the Ventricles contract and provide blood to the lungs & body. While traveling along this conduction system, the areas are differently depolarized and repolarized as seen in Figure 1.4. These electrical processes can be recorded through electrocardiography, producing an ECG. An ECG cycle is aligned in time with the action potentials at the bottom [32].

The ECG cycle as seen in Figure 1.5 consists of 3 phases, namely the P wave, the QRS complex, and the T wave. They correspond to the different phases of the heart. As seen in Figure 1.4, the P wave coincides with the depolarisation of the Atrium. Next, the QRS complex signifies the depolarisation of the Ventricles and the T wave is the repolarization of the Ventricles. The repolarization of the Atrium cannot be seen, it is overshadowed by the QRS complex [32].

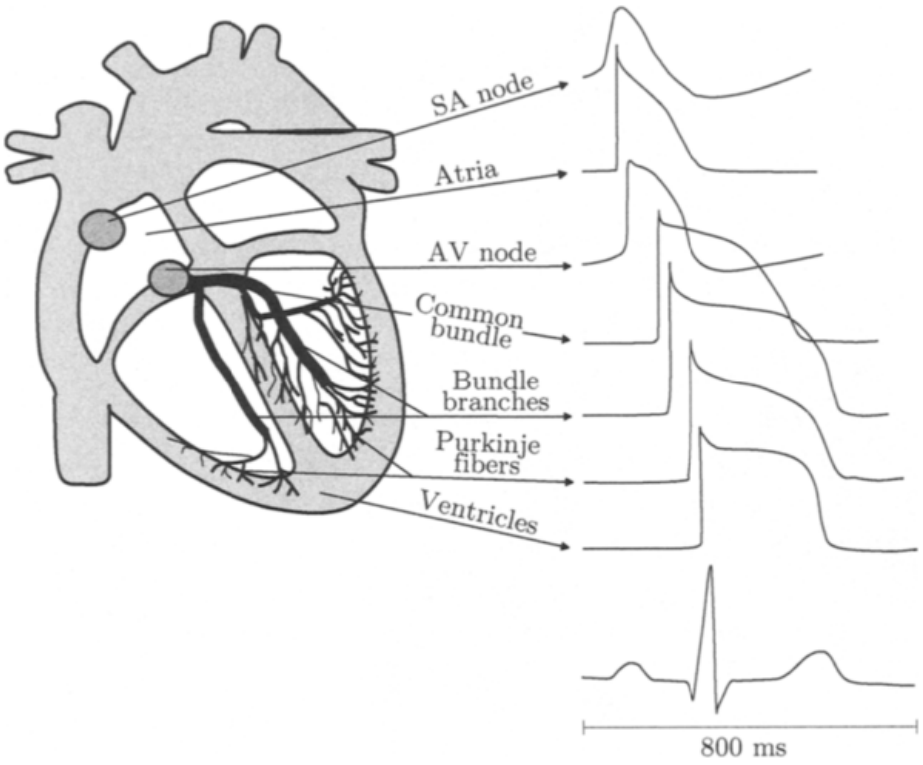

Figure 1.4: The heart conduction system with its action potentials and the correlating ECG heart cycle [32].

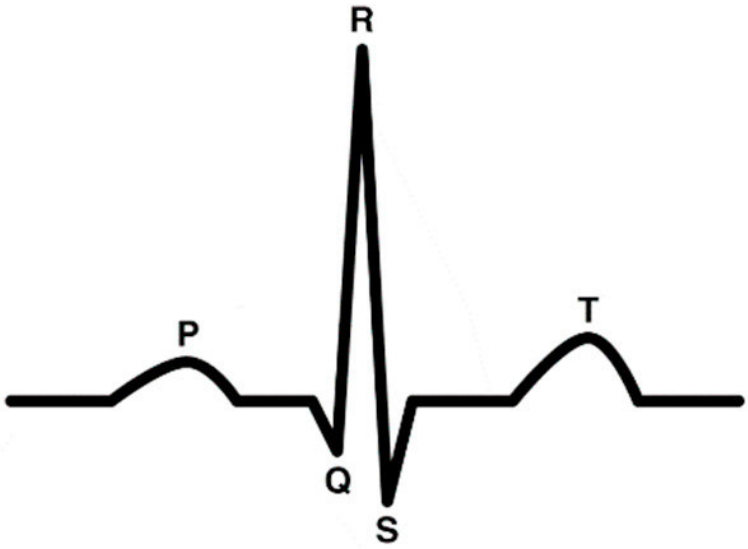

Figure 1.5: Typical ECG waveform of a cardiac cycle and its naming [33].

The QRS complex typically takes up 70 to 110ms, having a higher amplitude than the other waves. Its power spectrum (as seen in Figure 1.6) lies at a higher frequency, unlike the T & P wave. The frequencies shown are an approximate representation of the spectra. It is influenced by the participant examined, the lead measured and its origin [32].

There are various possible electrode constellations to measure an ECG. One of the simplest ECG electrode placements is the Einthoven Triangle. It utilizes 3 electrodes which provide 3 bipolar axes among each other. Their placement is on each hand and the right foot, creating a triangle in the process. The electrodes themselves can be measured as either unipolar or bipolar [32].

- **Unipolar leads** record the voltage of a single electrode against a reference electrode, giving information of whats in front of it.
- **Bipolar leads** measure differences between two electrodes, showing the voltage along their axis.

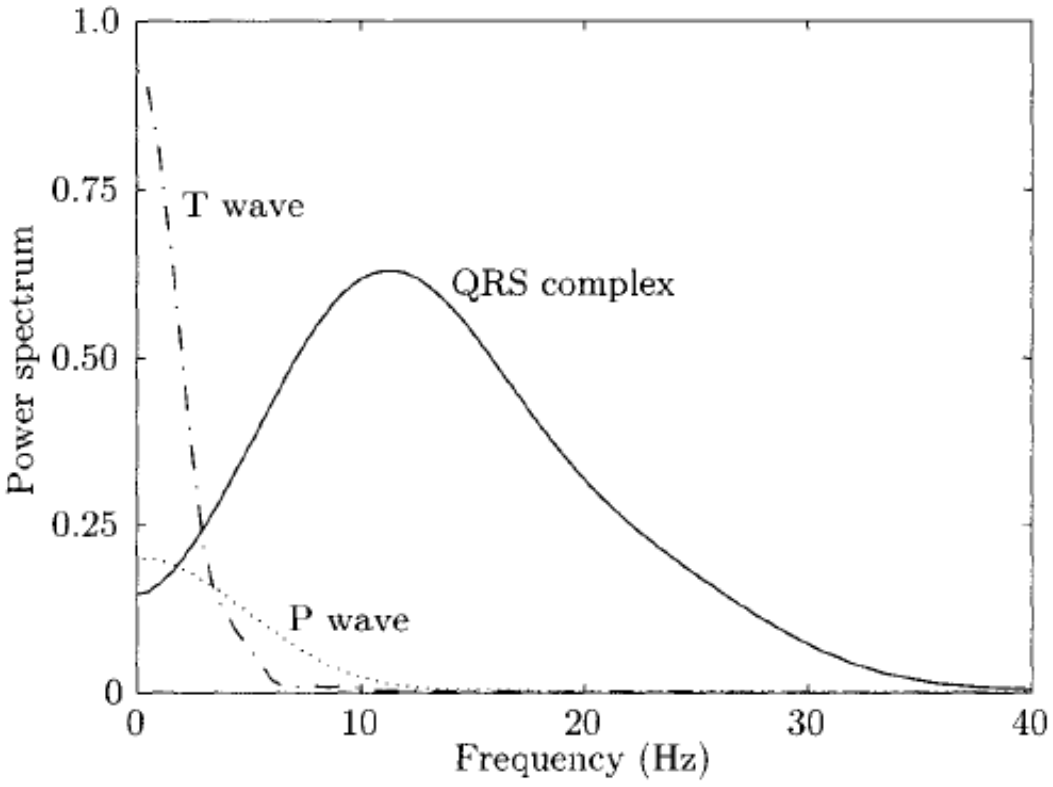

Figure 1.6: An approximate power spectrum of the frequencies of the ECG components [32].

Heart Rate Variability

The Heart Rate Variability (HRV) is a measure for variation in time intervals of heart cycles over defined periods. Successive heartbeats are compared for their time change. A measure to analyze its mean and standard deviation is to take NN intervals of normal heartbeats (SDNN). The bpm can change very drastically in a short period of time to compensate for physical activity or psychological challenges. Its purpose is to keep the body in a condition for optimum function. The mechanisms for HRV can be split up into 3 categories [34].

- long-term 24h
- short-term (approximately 5 min)
- ultra-short-term (<5min)

The long-term category represents slow-paced processes of the body, like the circadian rhythm. The ultra-short & short-term HRV is influenced by more fast-paced processes, like the PNS & SNS and respiration [34].

When the bpm increases/decreases, the heart cycle phases (seen in Figure 1.5) shift in time to accommodate. This can be perceived mainly at the T wave. Its occurrence can be up to 300ms after QRS complex for low bpm and will shift closer for higher bpm. The PQ and QRS have a low correlation in comparison [32].

1.2.2 Photoplethysmography

Photoplethysmography is a method to measure cardiac heart cycles through a light-emitting diode and a photodiode. Light at a defined wavelength is sent into the skin, as seen in Figure 1.7. Common wavelengths for the Light-Emitting Diode (LED) are red and infrared due to the high absorption by blood. It travels through the epidermis and dermis reaching down to the capillary bed. The light is absorbed and scattered along the way. Some of it is backscattered to the surface, reaching the photodiode. The blood volume at the location of measurement varies over a heart cycle, changing the diameter of the vessels. This change in blood volume affects the backscattering to the photodiode [31].

When the change in backscattering is plotted over time, the output takes the form of Figure 1.8. The signal is split into two phases, the anacrotic and catacrotic phase. The anacrotic phase is the upslope of the signal up to the systolic peak. It marks the systolic phase of the heart. From then on it is a falling edge showing the catacroctic phase which indicates the diastolic phase. Sometimes a dicrotic notch can be observed in the signal. It occurs because of the arteries reflecting the pulse wave in the periphery [35].

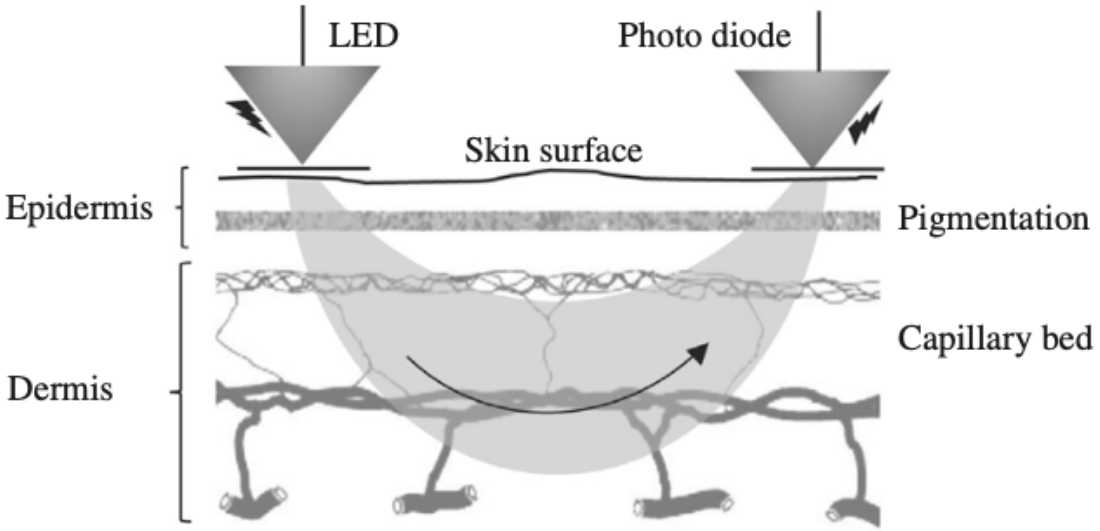

Figure 1.7: Structure of a PPG application with backscattering, adapted from [31].

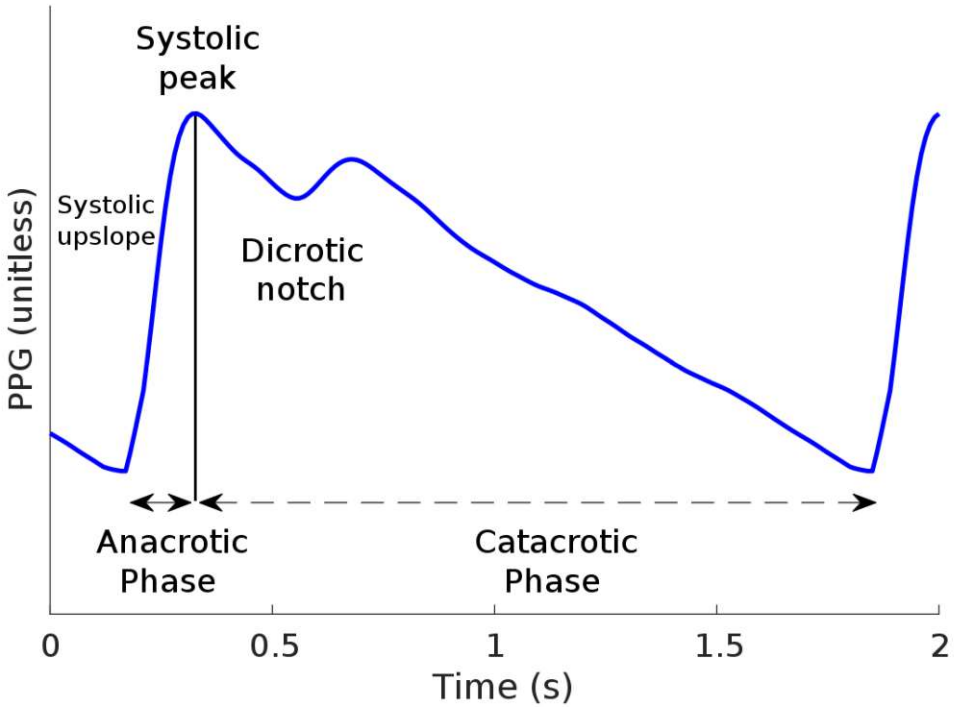

Figure 1.8: A blood volume waveform recorded by PPG, adapted from [35].

1.3 Closed-loop Auricular Vagus Nerve Stimulator Setup

The experimental setup for a closed-loop stimulation of the auricular Vagus Nerve is documented in the conference paper of Dabiri et al. [36]. The closed-loop stimulation observes the biosignals of the body and stimulates according to its rhythm, utilizing the auricular branch of the nerve. The structural components can be seen in Figure 1.9. Recording of the signals is done by the BIOPAC MP36 (BIOPAC Systems, Inc., CA, U.S.) with either Electrocardiography (ECG), Photoplethysmography (PPG), or Respiration. Its recording frequency is 500Hz, outputting 25 data points every 50ms. The analog output is converted to a digital signal by the DAQ NI6216 (National Instruments, Austin, Texas, U.S.) and sent to the PC. There the calibration and later on the online processing of the signal takes place. Via a serial port, the PC communicates with the microcontroller unit which is responsible for the stimulation of the auricular Vagus Nerve.

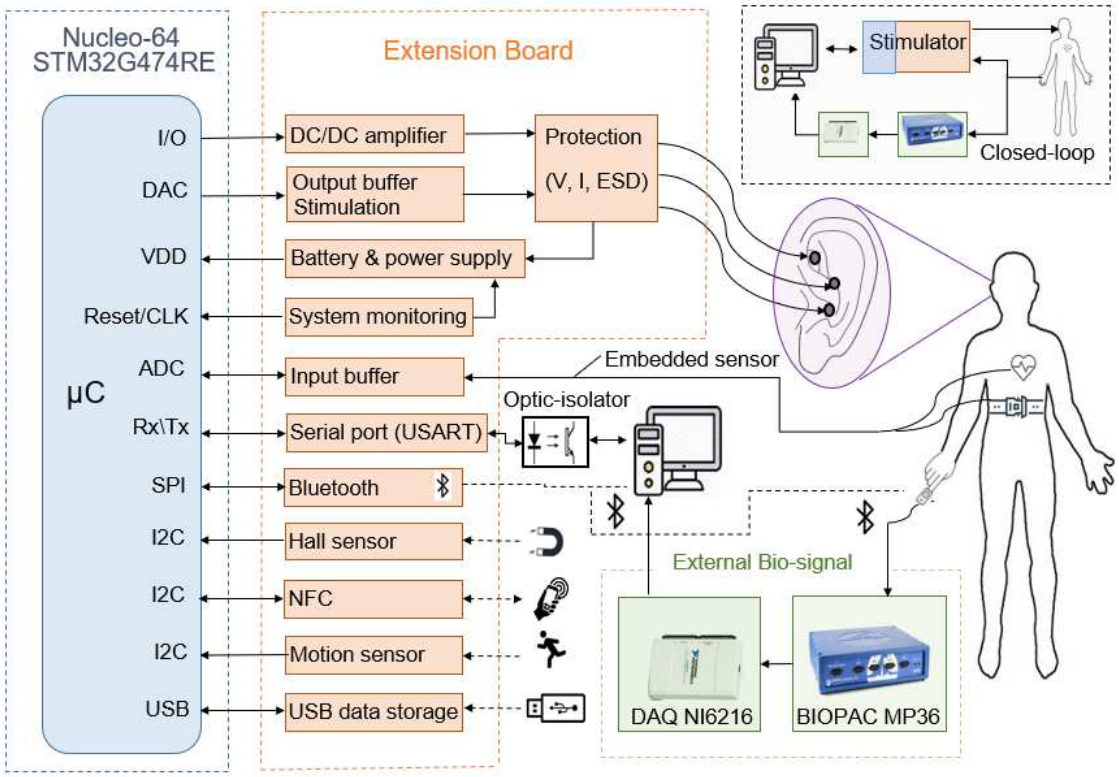

Figure 1.9: Experimental setup of a closed-loop auricular Vagus Nerve stimulation depicting the components [36].

The calibration happens by recording a 20s timeframe of the participant's biosignal and filtering it. After filtering, each cycle of ECG, PPG, or Respiration is cut up and the area of interest is identified. For ECG that would be the QR-slope. This slope is evaluated for every cycle and the interquartile range of 25 - 75% then serves as the reference for the actual stimulation. If the online ECG QR-complex is within this range, the setup will detect it and mark it as a peak. With this peak, the peak for the next ECG cycle can be predicted, providing a basis for timed closed-loop stimulation. Due to this flexible approach, the stimulator is capable of adjusting its pace to the heart rate variability (HRV) to a certain degree.

According to the paper [36], more than 90% of the biosignal peaks were identified with this approach. The accuracy was with a ±100ms standard deviation around the stimulation point of interest.

1.4 Integrated Sensor Module MAX86150

The MAX86150 is an integrated sensor module by Maxim Integrated, capable of measuring ECG and PPG. The required power supply for the chip is 1.8V, while the LEDs need 3.3V. During regular operation, the typical supply current is 400μA. When not needed, the MAX sensor can be sent to standby to save battery (0.7μA). The possible sampling frequencies range from 10 to 3200Hz for the PPG and from 200 to 3200Hz for the ECG. The ECG frequency band measures between 0.5 to 100Hz. If both ECG and PPG are being recorded, the sampling will be synchronized between the two [37].

In Figure 1.10, the internal layout of the module can be seen. The PPG section includes LED drivers that adjust the pulse width and amplitude of a red & infrared LED. Their backscatter as well as ambient light is captured by a photodiode. The ambient light is utilized in a proprietary light cancellation process by Maxim Integrated. The signal then ends up in an analog to digital converter (ADC) with a resolution of 19bit. Furthermore, an internal digital noise cancellation is implemented for power line signals at 50/60Hz and low frequency noise. The ECG is recorded via two electrodes through an Analog Front End to a 18Bit ADC. Both signals end up in the First In First Out (FIFO) data storage. The FIFO buffers data points for later retrieval, its content is emptied starting with the oldest entry. To communicate with the host and access the data an I^2C connection with 400kHz is implemented [37].

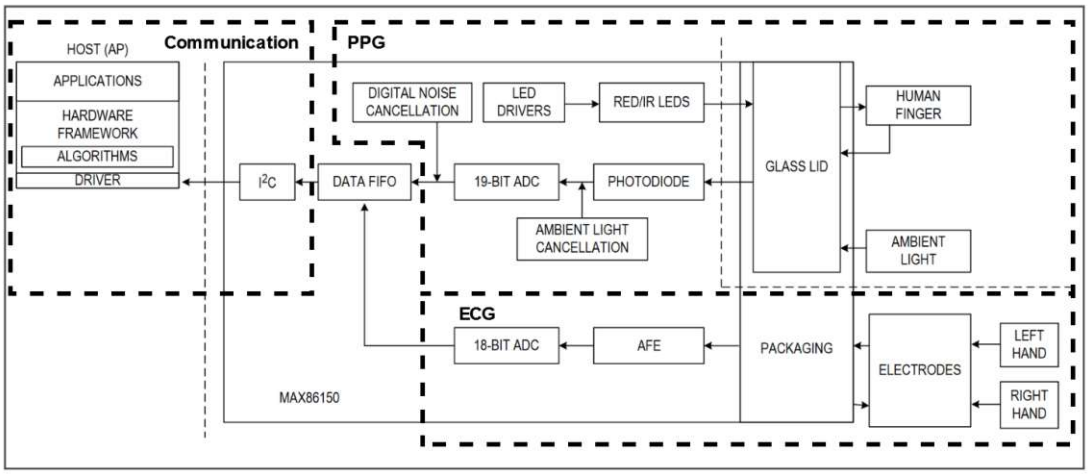

Figure 1.10: The schematic of the inner MAX86150 layout, adapted from [37].

I²C Interface

The I²C interface is a communication bus for data transfer via 2 wires. One wire establishes a mutual communication frequency. It is called Serial Clock Line (SCL). The other wire, the Serial Data Line (SDL), is pulled high or low to transfer a bit with each clock cycle of the SCL. There are 2 roles in the I²C setup [37].

- The master, initiating communication, sending commands or requesting data and establishing the SCL frequency.
- The slave, following the commands or providing data.

1.5 Objective

The current state of the art as described in Section 1.1.2 is an implanted VNS device, open and closed-loop. The project introduced in Section 1.3 aims to replace the need for implantation and facilitate the application through the closed-loop aVNS approach.

This thesis intends to replace the BIOPAC System as a biofeedback device in said closed-loop aVNS project. For the replacement, the integrated sensor module MAX86150 was chosen. It will be implemented for Electrocardiography and Photoplethysmography biosignal feedback. The BIOPAC replacement will provide portability to the experimental setup. The Nucleo-64 STM32G474RE Microcontroller Unit (MCU) will be utilized to read out the sensor, creating the need for reliable two-way communication to continually extract the data. The recorded ECG and PPG will be relayed to Simulink, MATLAB 2021b via a serial connection. Furthermore, this implementation necessitates adaptations or creation of communication, pre/post-processing, calibration, and filtering processes in the established platforms. Finally, the new stimulation setup will be analyzed, compared to the aVNS setup it is based on in terms of performance and discussed.

2 Methodology

The implementation is based on the established design by Dabiri et al. [36], as introduced in Section 1.3. For the remaining thesis, their experimental setup will be referenced as the BIOPAC Operating Stimulation Design (BOSD). The newly created setup for this thesis will be referred to as the Embedded Biosensor System/Stimulation (EBS).

As a first step to replacing the data acquisition of the BOSD, the new MAX86150 was configured appropriately. Next, the communication between all system parts (Sensor, MCU, and Simulink) was established and the data readout procedure was defined. To ensure data validity at all steps, measures were taken for data transfer reliability. All ECG measurements were taken at the thorax, while the PPG was measured at the finger of the participants. To utilize the sensor data, preprocessing steps were implemented in Simulink, and filters were designed to remove noise from various sources. The calibration was adapted to the new sensor by adjusting the cardiac cycle extraction and updating the templates for the validity check. It guarantees that a biosignal is present and if it is, parameters are calculated for the stimulation procedure. Next, the setup hardware delay was identified to ensure stimulation at the correct timepoint. To realize the closed-loop setup, the stimulation step size was adjusted to detect heart cycles more reliably. Furthermore, the stimulation voltage control was improved. Finally, the setup was evaluated by identifying the stimulation accuracy, the HRV influence, determining the maximum precision, and comparing it to the BOSD.

2.1 Data Acquisition

To introduce the MAX86150 sensor into the experimental setup, the sensor first needs to be configured with settings fitting the requirements. Next, the communication between all platforms was established and the data readout was defined. To provide a reliable data transfer between the MCU and Simulink, parameters are appended to the extracted data. In Simulink, the data is then checked and preprocessed for further application.

2.1.1 Sensor Configuration

For setup, Maxim Integrated has released recommended settings for the MAX86150. These recommended settings were studied and adjusted to the needs of the thesis project [38].

The registers in Table 2.1 are documented and explained in the following chapters. Furthermore, the recommended settings suggest setting the following, in the sensor documentation

unmentioned, registers as seen in Table 2.2 [38]. These set up the Analog Front End to optimize the ECG recording. We implemented them as proposed. To differentiate between the addresses of the registers and the hex codes to be written into the registers, the addresses will be written with an "&" in front. A detailed breakdown of all mentioned registers is shown in the Appendix.

Table 2.1: MAX86150 Registers with their addresses and the values to be written.

Register	**Address**	**Written**
System Control	&0x0D	0x01
		0x04
FIFO Configuration	&0x08	0x10
Data Control	&0x09	0x92
LED2 PA	&0x12	0x55
PPG Configuration 1	&0x0E	0xDF
PPG Configuration 2	&0x0F	0x18
ECG Configuration 1	&0x3C	0x01
ECG Configuration 3	&0x3E	0x0D

Table 2.2: MAX86150 Registers with their addresses and the values to be written for the Analog Front End ECG setup.

Register	**Address**	**Written**
Undefined Naming	&0xFF	0x54
	&0xFF	0x4D
	&0xCE	0x0A
	&0xCF	0x18
	&0xFF	0x00

System

As a first step, the MAX86150 is reset by setting the **System Control register** (&0x0D) with "0x01". Next, the FIFO_EN in the register is set with "0x04" to enable the sensor to push its data into the FIFO data storage unit.

When the FIFO is enabled, it needs to be set up in the **FIFO Configuration Register** (&0x08). FIFO_ROLLS_ON_FULL is activated by setting the register to "0x10", the rest is left as is. This causes the chip to overwrite its oldest data point if the maximum storage capacity of 32 samples is reached.

Next, the desired sensors are assigned to the **Data Control Registers** &0x09 and &0x0A. The Data Control Registers can be populated with hex numbers corresponding to sensors. For PPG measurements "0x01" signifies an infrared LED and "0x02" is a red one, while "0x09" enables ECG recordings. Each Data Control Register can hold up to 2 sensor hex numbers. For this project, two sensors were chosen. For PPG the red LED (0x02) and the ECG (0x90) by setting the Data Control Register &0x09 to "0x92".

PPG

The **LED2 PA Register** (&0x12) is responsible for the current of the LEDs. The higher the value, the stronger pulse amplitude. The recommended settings state 17mA, a hex of "0x55".

The **PPG Configuration 1 Register** (&0x0E) is written with "0xDF" and has 3 parameters.

- PPG_LED_PW defines the pulse width of the LEDs and is set to 400 microseconds LED pulses.
- PPG_SR is the sample rate control determining the sampling frequency of the chip. A frequency of 800 Hz was chosen.
- PPG_ADC_RGE is the ADC control range for the LED. The recommended setting suggests a resolution of 62.5pA.

For the **PPG Configuration 2 Register** (&0x0F) the documentation provides an SMP_AVE option to average neighboring samples and reduce the throughput. The recommended settings ignore this option and propose "0x18" as an unlisted option, explaining it with "for 20µs delay from the rising edge of the LED to the start of integration" [38]. We adopted this recommendation.

ECG

The **ECG Configuration 1 Register** (&0x3C) is responsible for the sample rate. By setting it to "0x01", the frequency is defined as 800 Hz.

For the **ECG Configuration 3 Register** (&0x3E), the data sheet suggests "0x0D" for a PGA_ECG_GAIN of 8 V/V and IA_GAIN of 9.5 V/V.

2.1.2 Communication

Communication between the MCU and the MAX is provided by the I^2C connection with a frequency of 400 kHz. A pull-up with 5V was implemented to communicate over the SDA and SCL lines. Interrupts by the sensor module are available, but currently unused. For data retrieval, a Direct Memory Access (DMA) was established, which extracts data directly without involving the processor.

Between the MCU and the PC, a universal asynchronous receiver-transmitter (UART) was implemented for serial communication. It is set up with a baud rate of 115200, 1 stop bit, 8 data bits, and no parity.

2.1.3 Data Readout

The FIFO data storage is restricted to 32 samples per sensor. Considering a sampling frequency of 800Hz, the readout needs to happen at least every 40ms to avoid an overrun and data loss. This was done by creating an interrupt on the MCU side and initiating data extraction. For the interrupt, the prescaler and counter period were chosen as 4800 and 250 respectively. The MCU runs at a 48MHz clock frequency. Therefore, the DMA is called every 25ms during which the FIFO amasses 20 data points.

$$\frac{48.000.000Hz}{4.800 * 250} = 40Hz$$

The ADC measures with a resolution of 18-bit for ECG and 19-bit for PPG. For this reason, every ECG and PPG data point takes up 3 bytes, as seen in Figure 2.1.

	FIFO_DATA																							
	BYTE 1								BYTE 2								BYTE 3							
ADC Resolution	FIFO_DATA[23]	FIFO_DATA[22]	FIFO_DATA[21]	FIFO_DATA[20]	FIFO_DATA[19]	FIFO_DATA[18]	FIFO_DATA[17]	FIFO_DATA[16]	FIFO_DATA[15]	FIFO_DATA[14]	FIFO_DATA[13]	FIFO_DATA[12]	FIFO_DATA[11]	FIFO_DATA[10]	FIFO_DATA[9]	FIFO_DATA[8]	FIFO_DATA[7]	FIFO_DATA[6]	FIFO_DATA[5]	FIFO_DATA[4]	FIFO_DATA[3]	FIFO_DATA[2]	FIFO_DATA[1]	FIFO_DATA[0]
PPG (19-bit)	x	x	x	x	x																			
ECG (18-bit)	0	0	0	0	0	0																		

Figure 2.1: ADC resolution for ECG and PPG with corresponding bit alignment [37].

Therefore, the DMA reads out two sensors producing 20 data points with 3 bytes each. In total 120 bytes are retrieved every 25ms.

To extract the stored data out of the FIFO Data Register (&0x07) it is first determined where in the register the first data point is located. This is realized through reading three registers starting with FIFO Write Pointer (&0x04), Overflow Counter (&0x05), and ending with FIFO Read Pointer (&0x06).

- Overflow Counter shows how many samples were overwritten.
- FIFO Write Pointer signifies the location where the next data point is written.
- FIFO Read Pointer shows the location of the oldest data point.

Through subtraction of the write and read pointer, it is determined how many data points need to be retrieved. If the Overflow Counter states data points were lost, the FIFO is full and needs to be cleared.

2.1.4 Data Transfer Reliability

When the data is extracted it will be transferred from the MCU to the PC by UART. Simulink picks up the data by a serial receive.

Before the transfer takes place, additional parameters are appended.

- Initiator ("st") and Terminator ("\r\n")
- HAL_tick() to ascertain the timepoint of readout
- FIFO data amount read during this cycle
- Cyclic redundancy check (CRC) is performed and added.

Initiator and Terminator signify the beginning and end of the relevant data to be read out by Simulink. The CRC ensures the validity of the data after transfer.

The CRC is calculated by adding up all the data point bytes of the measurement. A sum of 120 bytes is created, but the CRC is only represented by one byte (uint8_t) with a maximum of 255. When this value is exceeded during adding, the counter starts again from 0. This leads to a modulo operation with a base of 256. The remaining rest after the calculation is the checksum value appended.

After concatenation, a total of 140 bytes get sent. This includes the 120 bytes of data, 4 bytes Initiator & Terminator, 4 bytes timestamp, 1 byte stating the number of samples read, and 1 byte CRC. The remaining 10 bytes were kept open for future use.

The reliability of data transfer between the MCU and Simulink was investigated by recording data and counting the lost bytes over the duration. This was done by checking the CRC value and subsequently the recorded number of samples in the data package in question.

2.1.5 Simulink Preprocessing

The upper graph in Figure 2.2 depicts the steps taken in the experimental setup. The data is acquired by the sensor and retrieved by the MCU. Next, Simulink evaluates the data and sends a command to the stimulator for stimulation. To use the data in Simulink, a preprocessing step is undertaken. It receives and prepares the data for further evaluation.

These reception and preprocessing steps are visualized in the lower section of Figure 2.2. The Serial Receive block was configured to expect a data package of size 140 every 25ms from the MCU. It is then forwarded to be saved into the workspace for analysis and split between data points and appended parameters.

For the data, the CRC checksum is generated once more and compared to the previous CRC value contained in the parameters (see Section 2.1.4). If they are the same, the data is valid. Otherwise, a transmission error took place and the data points will be invalid.

Simultaneously, the data string is formatted into 20 data points with 6 bytes, 3 for each PPG and ECG. To extract the value, these 3 bytes need to be bit shifted into a single uint32/int32. The bytes are concatenated in the way Figure 2.1 visualizes them. ECG data can be negative and the conversion is achieved through the two's complement. The signal can be multiplied by $1.6114 \cdot 10^{-4}$ to rescale the ADC values to mV. The PPG values do not need to be adjusted.

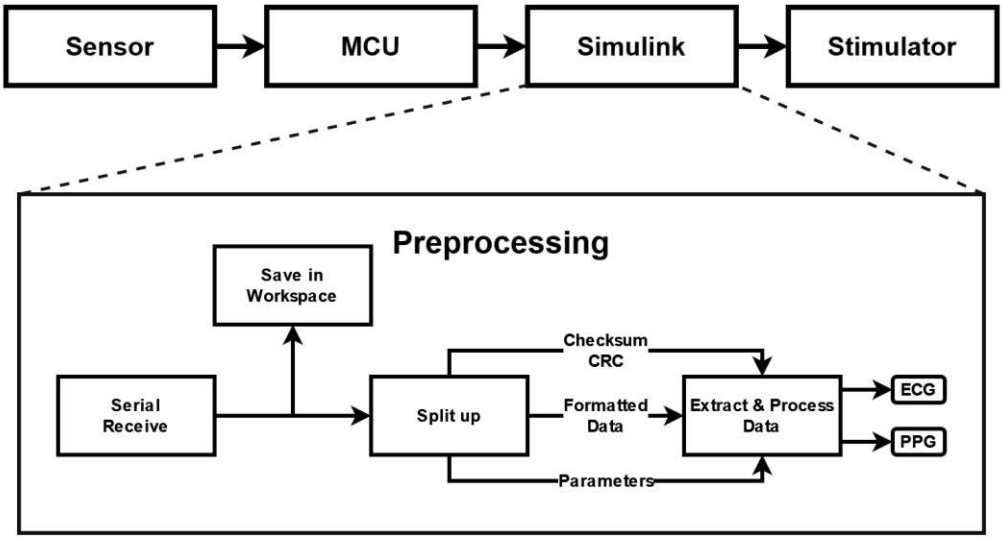

Figure 2.2: Block illustrating the preprocessing steps of ECG & PPG data in Simulink.

2.2 Digital Filter Design

The signal provided by the MAX86150 needs filtering to remove the noise of, among others, the power line. This was done with two filters. The design was kept similar to the established design with BIOPAC as its signal source.

For the stimulation and real-time signal processing of an ECG, a lowpass filter was needed. Several filters were designed and investigated in 10-minute test runs with the setup. The examined parameter was the capability in identifying the QRS complex correctly. The main two investigated filters were lowpass Bartlett Hanning Window FIR filters. One with an order of 140 and a cutoff frequency of 5Hz, the other with an order of 112 and 6Hz (as seen in Figure 2.3). Additionally, for calibration purposes as well as postprocessing, a bandpass filter was implemented with an order of 300 and cutoff frequencies of 1Hz and 20Hz.

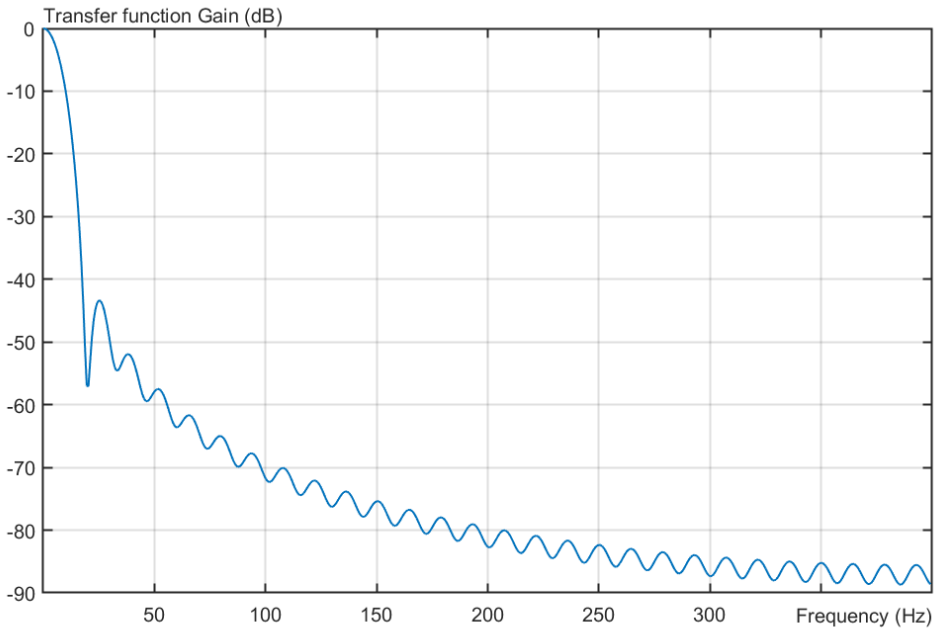

Figure 2.3: FIR filter with a Bartlett Hanning Window Lowpass, Order 112 and Cutoff frequency 6Hz.

For the remaining project, the lowpass with order 112 and a cut-off frequency of 6 Hz is utilized for descriptive purposes. The PPG processing utilizes the same lowpass filter as the ECG setup for stimulation. The simpler structure of the signal eliminates the need for a bandpass in PPG for pre/post-processing.

FIR filter provides a steady group delay in the time domain. For the 112 order filter, this leads to a delay of 56 samples and for the 300 it is 150 samples. To compensate for the delay, the time needs to be adjusted by $\frac{56}{800Hz} = 0.07s$ and $\frac{150}{800Hz} = 0.1875s$ respectively.

FIR filtering produces a step response at the beginning of the signal that needs to be compensated. To avoid the step response, approximately as many old data points are buffered as the number of orders in the filter. These old data points are then added in front of the new data. After filtering, the old data, that is affected by the step response is cut. The remaining data is unaffected and can be used for further steps. For the stimulation, the last 130 data points are buffered and filtered in addition to 20 new ones. 110 are cut and only the last 40 (50ms) are utilized for the next steps. Both, ECG as well as PPG use this approach.

2.3 Calibration

The calibration process of the BOSD setup was adjusted to the new sensor. This was done by creating a new ECG & PPG template. Furthermore, the cutoff points for ECG & PPG cycle extractions were investigated with a fixed starting point. The starting and cutoff point define a frame for data point extraction. This frame is applied for each cardiac cycle of ECG & PPG. Starting and cutoff points are illustrated in Figure 2.4. The BOSD peak detection algorithm was tested and improved.

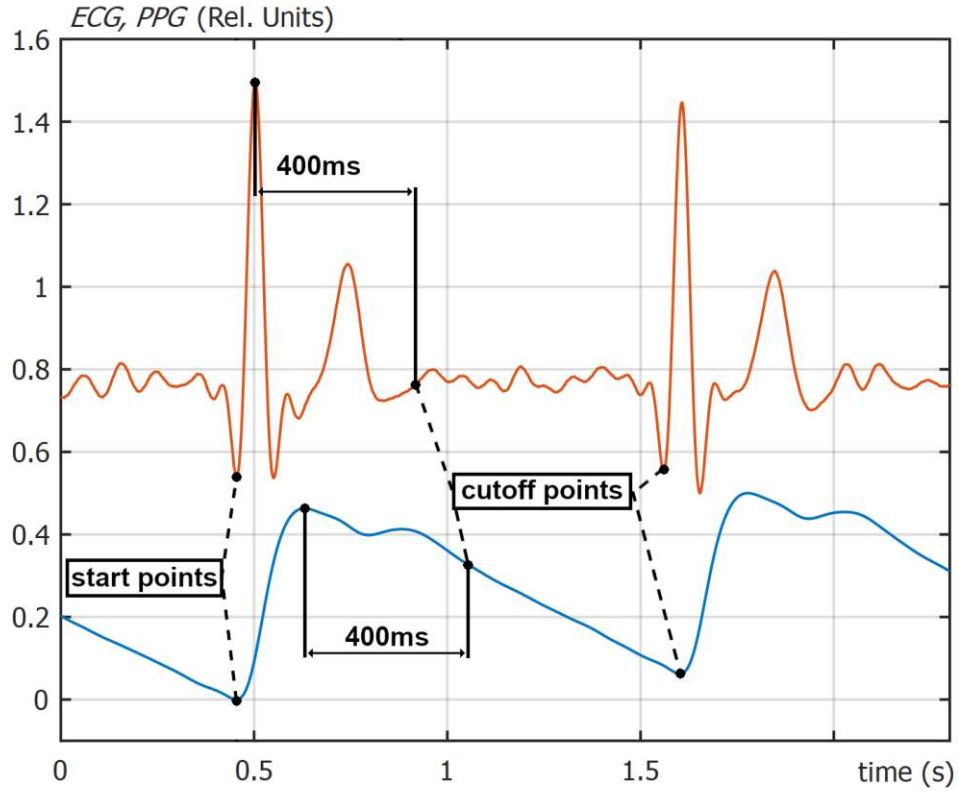

Figure 2.4: ECG and PPG cycles with a fixed starting point and variable cutoff points.

As a first step during the calibration, the signal is duplicated and filtered with either the bandpass or the lowpass. The bandpass signal is used for the following calibration steps. The lowpass signal will be read out during the parameter calculation for the stimulation threshold (see Section 2.3.4).

2.3.1 Cardiac Cycle Extraction

During calibration, each cardiac cycle is identified by finding its peak. For ECG it is the R peak that will be detected. To determine the approximate distance between R peaks utilized by the find peaks function, a preselection prompt was introduced. It prompts the user to mark an undefined number of R peaks, as seen in Figure 2.5. Their mean distance multiplied by 0.8 will be output. Previously, a standard distance of 0.5s was implemented. Going outward from the detected R peaks, the corresponding Q and S peaks are identified. As a next step, each cycle is cut out, the start point being the Q peak. Possible endpoints/cutoffs are 400ms after the R peak or the next Q peak, as seen in Figure 2.4.

For PPG, peak detection identifies the systolic peak. The same preselection prompt is applied for PPG for distance identification. To find the onset of the PPG cycle, the minimum to the left of the peak is taken. This minimum is the starting point for extraction and the endpoint is either 400ms after the peak or the next onset (as seen in Figure 2.4).

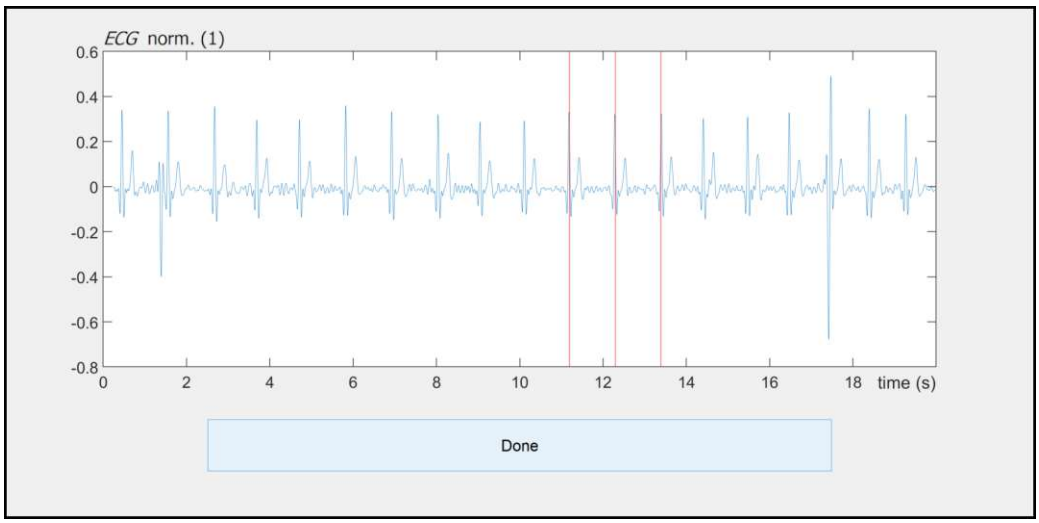

Figure 2.5: Application plot prompting the user to mark R peaks for distance approximation.

2.3.2 Validity check

After extracting each cycle, a validity check of the data is performed. To do so they are resampled to a common size of 256 data points and normalized in amplitude. A cross-correlation is then executed with the resampled cycle and a template created to be a typical ECG or PPG cycle of the MAX86150. The cross-correlation is defined as seen in Equation 2.1 and ranges from -1 to 1 [39]. The correlation coefficient $\hat{p}_{ij}$ is calculated from N elements of two data sets x_i & x_j and their respective means $\bar{x}_i$ & $\bar{x}_j$. If the correlation coefficient falls below 0.65, the wave will be disqualified by the setup. The calibration fails if more than 25% disqualify.

$$\hat{p}_{ij} = \frac{\sum_{t=1}^{N}[(x_i - \bar{x}_i)(x_j - \bar{x}_j)]}{\sqrt{\sum_{t=1}^{N}(x_i - \bar{x}_i)^2 \sum_{t=1}^{N}(x_j - \bar{x}_j)^2}} \tag{2.1}$$

2.3.3 Template Creation

To create the ECG template, a recording of 423 seconds was made, with the participant seated at rest. Each cycle was extracted, resampled to 256, and superimposed. For the typical template, the median was taken for each data point. The same was done for the PPG template with a recording of 396 seconds, seated at rest.

For the cardiac cycle extraction of PPG and ECG, a start point and endpoint/cutoff need to be chosen. It is imperative to choose the same as in Section 2.3.1, Cardiac Cycle Extraction. The start points were the Q peak (ECG) and the onset of the rising edge of the PPG.

The influence of the endpoints on the calibration was investigated with a cutoff at 400ms after the R peak and at the next cycle at the Q peak for ECG (marked ECG cutoff points in Figure 2.4). For PPG 400ms after the systolic peak and at the rising edge of the systolic peak of the next heart cycle (marked PPG cutoff points in Figure 2.4). Biosignal recordings were undertaken at approximately 60bpm and 100bpm for PPG and ECG over 20 seconds. For these recordings, the calibration process was applied and the cross-correlations were calculated to ascertain the effect of the different cutoffs.

2.3.4 Parameter Calculation

If the cross-correlation is successful, the necessary parameters for stimulation are calculated.

- QR complex slope
- Systolic peak rising edge slope
- Mean cycle interval for ECG/PPG

The slopes of the QR complexes of each cycle define the threshold for real-time peak detection. To extract them, the Q and R peaks identified in Section 2.3.1 are taken over from the bandpass filtered signal to the lowpass signal that is actually used during stimulation. Each QR slope gets linearly interpolated. The first quantile is then multiplied by 0.6 to ensure inclusion. This value defines the lowest rising edge of an ECG cycle accepted as a QR slope. The same procedures apply for the cycle extraction of the PPG. Its wave onset to the systolic peak is linearly interpolated for the lowpass/stimulation filtered signal. The first quantile is rescaled to 0.7 instead.

The distances between R peaks and Q peaks of the following heart cycle are identified. For the PPG it is the systolic peak to the onset of the next cycle. Their medians define the time (t_{RQ} for ECG) to wait after slope identification for stimulation.

2.4 Latency

Several steps need to be undertaken until the patient is stimulated. During these steps (seen in Figure 2.6) a latency is introduced, called the hardware delay. It can be roughly broken up into 3 components:

$$t_{\text{HardwareDelay}} = t_{\text{Communication}} + t_{\text{Processing}} + t_{\text{Stimulation}} \tag{2.2}$$

Interfacing between the sensor, MCU, and Simulink is represented by $t_{\text{Communication}}$ (I^2C & UART). The $t_{\text{Processing}}$ step includes handling and evaluating the data (e.g. Parameter creation, Filtering, Slope Detection, etc.). The stimulation application step after command reception is characterized by $t_{\text{Stimulation}}$.

The sequential order of the steps in Figure 2.6 starts with the MAX86150 integrated sensor recording the biosignals. The sensor collects a total of 20 data points before transferring them. The transfer happens through I^2C. The MCU creates and evaluates parameters before forwarding the data to Simulink via a serial/UART connection. Simulink processes the data, filters it, and deduces if a QR slope or PPG slope is present. If a slope is detected, it sends a command via serial to the stimulator/MCU for a stimulation initiation. The stimulator evaluates the command and applies the stimulation.

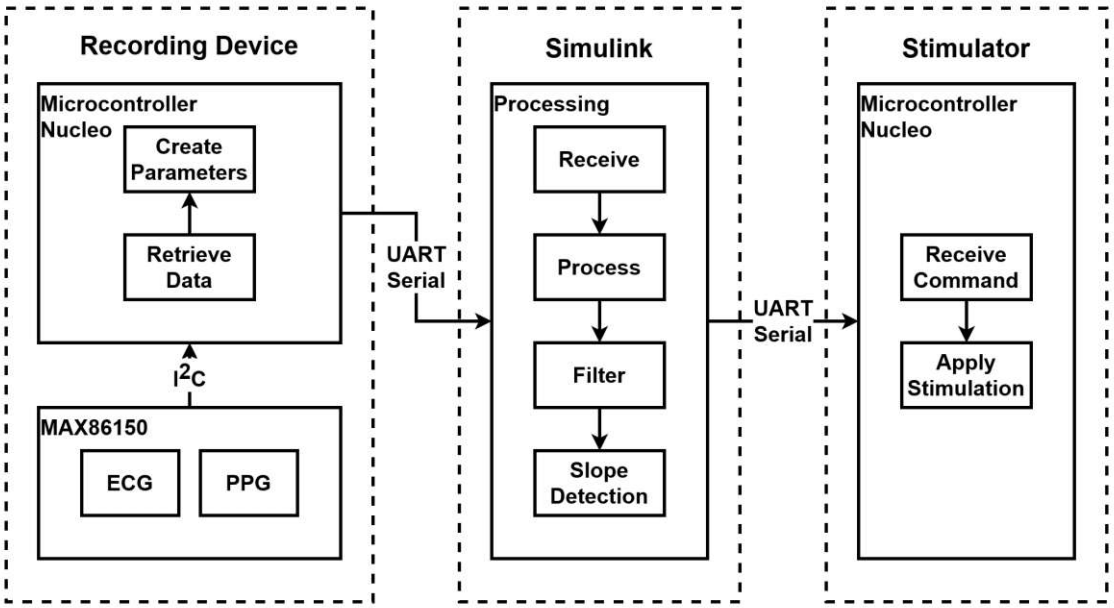

Figure 2.6: EBS setup steps from recording to stimulation.

For the stimulation, the setup aims from the current R peak to the next Q peak. Figure 2.7 illustrates this predicted distance as t_{RQ}. Due to $t_{\mathrm{HardwareDelay}}$ an unknown amount of milliseconds has passed already when the QR slope is seen by the experimental setup. An example of a hardware delay is depicted in Figure 2.7. If the predicted distance was adhered to, the stimulation timepoint would be shifted behind from the target point by the amount of the hardware delay. To compensate, the delay is subtracted from the predicted distance giving us the actual time delay ($\triangle t_{\mathrm{Delay}}$).

$$\triangle t_{\mathrm{Delay}} = t_{\mathrm{RQ}} - t_{\mathrm{HardwareDelay}} \tag{2.3}$$

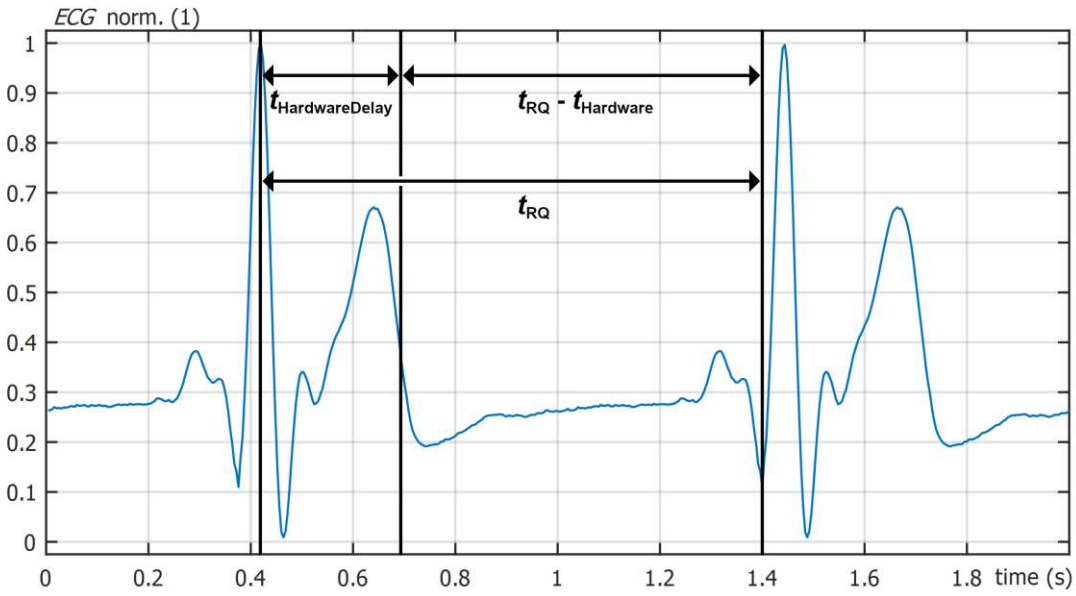

Figure 2.7: ECG cycles with a predicted time distance between the R & Q peak. Additionally, an example of a hardware delay is depicted, showing the time that might have passed already. The subtraction between the two illustrates the corrected prediction distance.

To investigate the hardware delay, recordings were made as seen in Figure 2.8. A participant was directly connected to a BIOPAC system via ECG, depicted in blue. Simultaneously another ECG was acquired by the EBS setup with the MAX86150. The EBS setup (ECG in red) was set up with $t_{\mathrm{RQ}} = 0$ and $t_{\mathrm{HardwareDelay}} = 0$ to immediately send a command to the MCU for stimulation if it detects a QR complex. Instead of stimulating the participant, the BIOPAC system records the pulse. By subtracting the R-peak in BIOPAC and the onset of the stimulation pulse, the hardware delay was deduced.

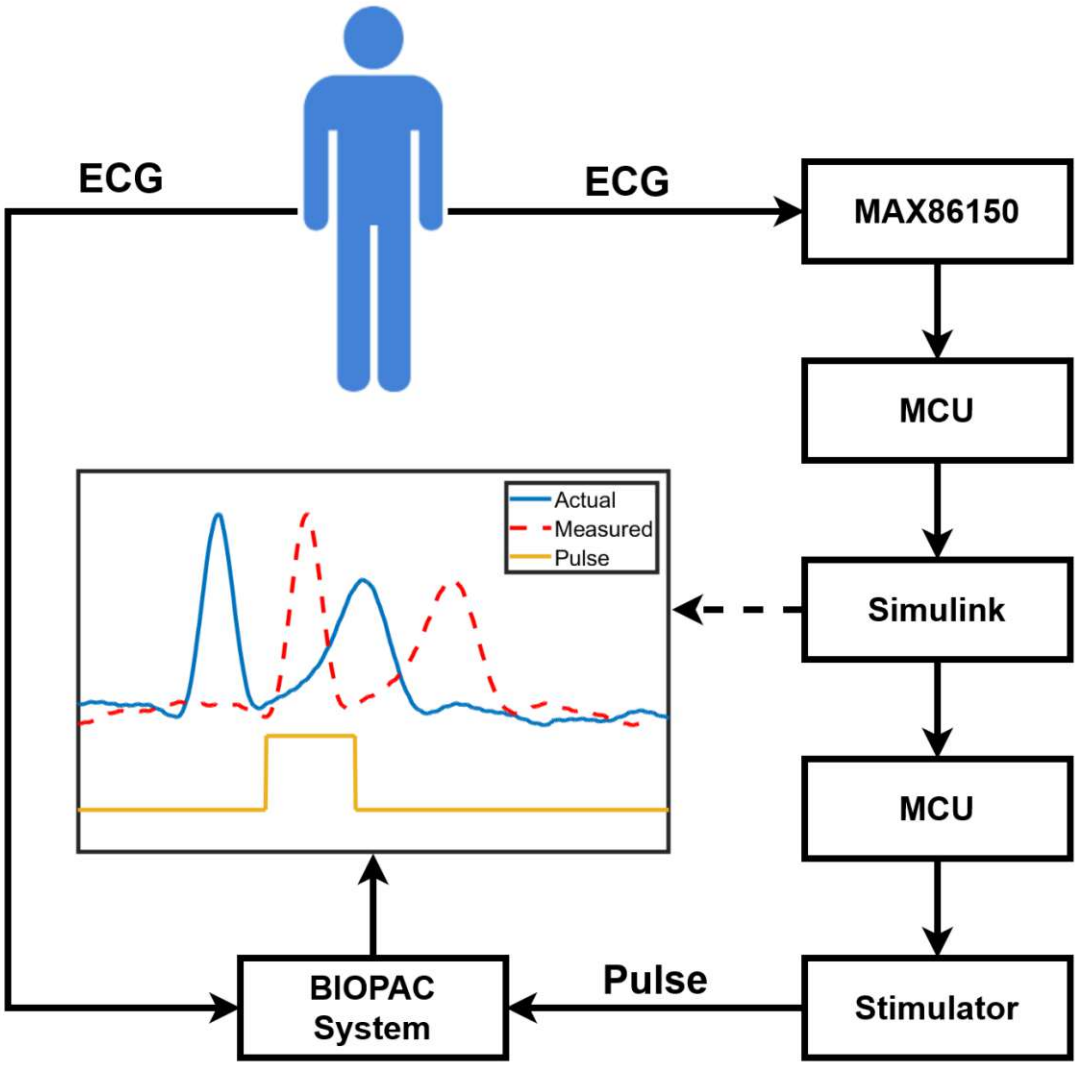

Figure 2.8: The VNS setup based on the EBS with the MAX86150 sensor is depicted. Whenever Simulink (red) detects a heart cycle, it immediately sends a command to stimulate. The stimulation pulse is applied to the BIOPAC System. Simultaneously, the BIOPAC System is fed a direct ECG (blue). The latency offset can be observed as the difference between the BIOPAC R peak and stimulation pulse onset.

2.5 Closed-loop Realization

The closed-loop process is visualized in Figure 2.9 and described based on the ECG. Simulink takes timesteps in the size of 1.25ms. It expects a data package from the recording device every 25ms and checks the serial receive. If data arrives, it is filtered and the slope is detected by linear interpolation of a 50ms data window (seen in Figure 2.10). During the calibration process, the current distance between cardiac cycles is evaluated. If the QR slope is detected, the timepoint of the R peak will be recorded. Starting with this R peak, the algorithm waits for the next cardiac cycle, based on the calibration time, to stimulate during a selected phase. The stimulation is controlled through a start and stop command sent to the MCU.

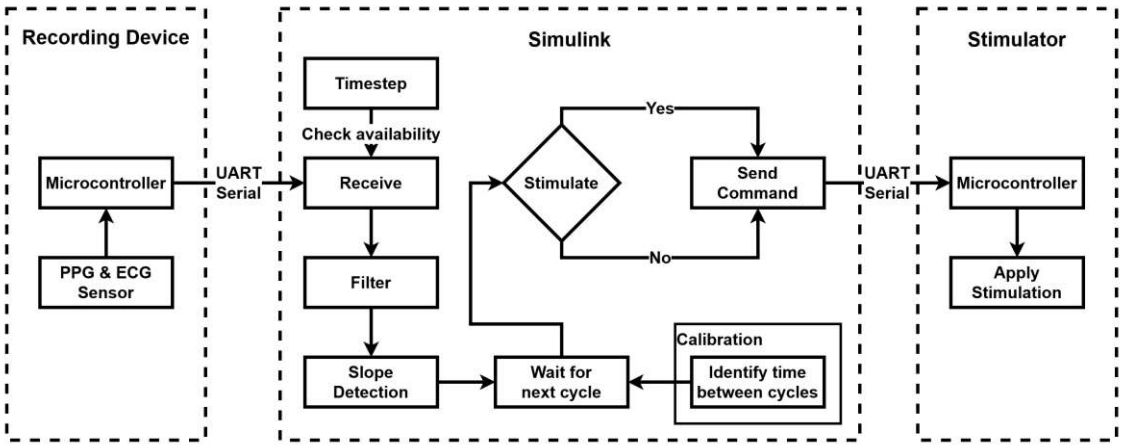

Figure 2.9: Closed-loop VNS based on the EBS setup. The basic workflow of the recording device, Simulink and the stimulator setup are depicted.

2.5.1 Stimulation Step Size

The timeframe for interpolation consists of a 50ms window. For an 800Hz recording frequency, this produces 40 data points. A lowpass filtered ECG signal fragmented into windows of 50ms with 50ms steps can be seen in Figure 2.10. Each window is linearly interpolated.

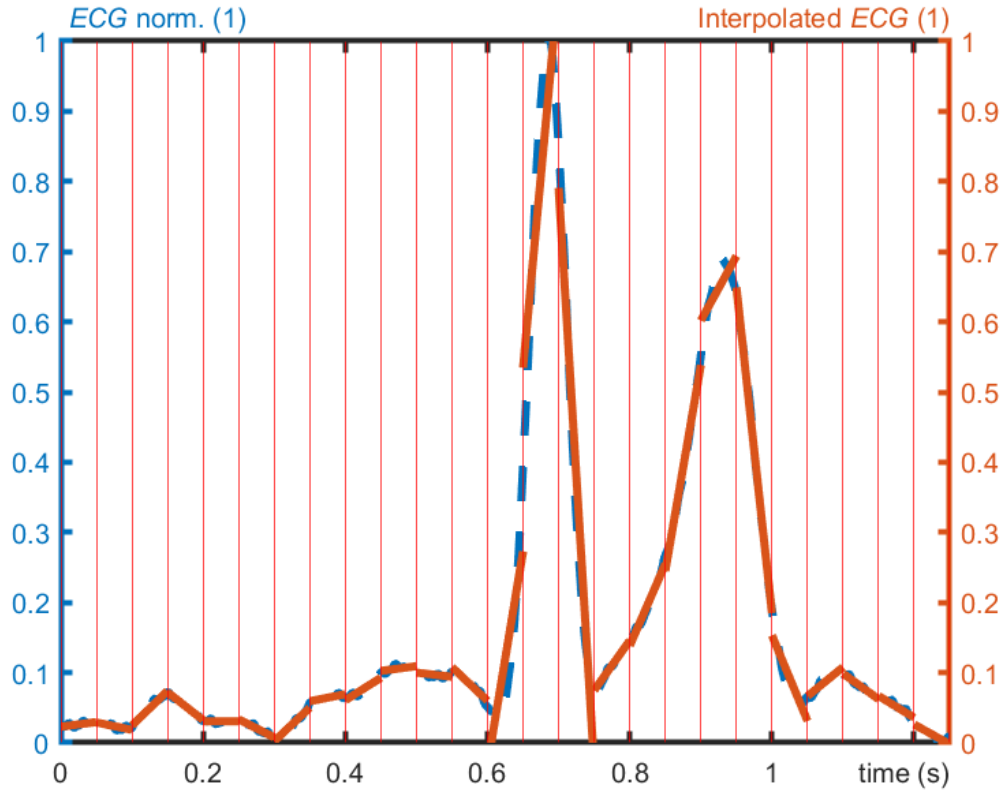

Figure 2.10: Linear interpolation of a lowpass filtered ECG signal with a 50ms step size and windows.

The 50ms step size was investigated for ECG to ascertain the detection efficiency. For this purpose, the step size was reduced to 25 ms for comparison. To retain the time-frame/window of 50ms, each interpolation shares 25ms/20 data points with the previous one. Furthermore, the detection precision of the QRS complex was investigated for both step sizes. The participant was connected to the setup and recordings were made consecutively for approximately 10 minutes with each setup.

2.5.2 Stimulation Voltage Control

After an identified QRS complex, Simulink will send a command via UART to the stimulator to initiate a stimulus. This command was adjusted from a 1 letter + 2 digits to a 1 letter + 4 digits command. The letter can be either an "s" for starting or an "f" for stopping the stimulation. The digits define the applied voltage if the stimulation is active. The four digits allow for voltage changes of 1 millivolt in the range of 50-3000mV.

2.6 Setup Evaluation

After the completed implementation, the performance of the EBS setup was evaluated. First, the accuracy of the Simulink prediction was compared with the actual time of stimulation. Then, the influence of the HRV on the stimulation precision was examined and the maximum in precision was determined. Lastly, a performance comparison was made between the newly created EBS setup and the BOSD setup.

2.6.1 Stimulation Accuracy

To ascertain the accuracy of the EBS setup a measurement was taken as described in Section 2.4 and illustrated in Figure 2.8. This time with the identified latency implemented. The predictive timepoint of stimulation according to Simulink was evaluated against the actual stimulation measured by the BIOPAC System. The resulting distributions were statistically evaluated and compared.

2.6.2 HRV Influence

The HRV as an influencing factor on the predictive stimulation distance and resulting precision was investigated. Furthermore, the best possible precision in stimulation around the point of interest was analyzed. The BIOPAC recording from the previous Section 2.6.1 was used. For every heartbeat stimulated, the HRV and the distance between predicting peak and stimulation onset were calculated.

2.6.3 Performance Comparison

To determine the performance, the EBS was compared to the BOSD. The measurement was set up as seen in Figure 2.11. The main difference in setup lies in the exchange of the BIOPAC system and ADC with the MAX86150 & MCU as a biofeedback source. Furthermore, all changes/improvements in the EBS setup undertaken over the course of this thesis were implemented as well. A participant was connected via ECG to both setups and the calibration as well as the stimulation were performed in synchronization. In the postprocessing, the amount of correctly identified cycles and the prediction accuracy were analyzed.

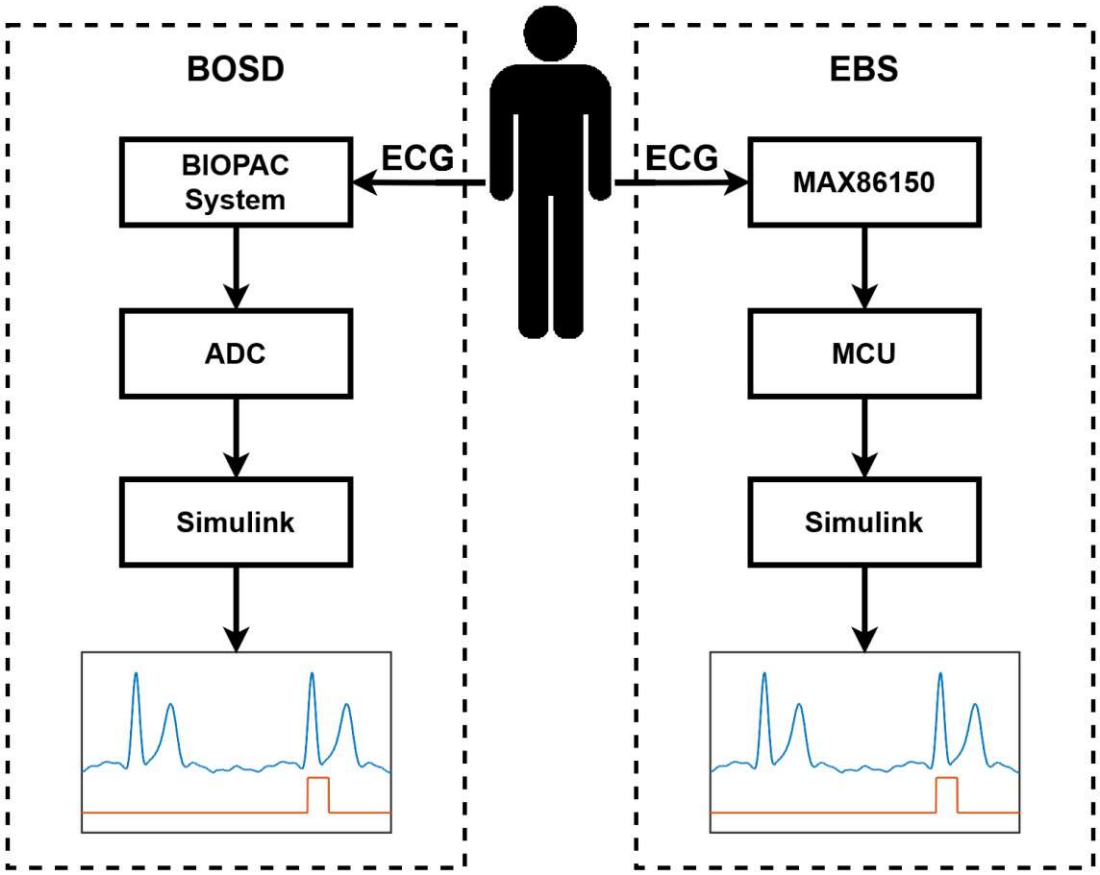

Figure 2.11: Two vagus nerve stimulation setups (BOSD and EBS) targeting a common point in their respective ECG signal by prediction from the previous heart cycle. By applying them simultaneously, their stimulation distributions can be evaluated and compared.

3 Results

In this section, the findings of replacing the BIOPAC System (BOSD) as a feedback device with the MAX86150 sensor (EBS) are disclosed. Beginning with the data lost during the process. Next, the utilized filter for preprocessing to extract the cardiac cycles, calibrate and create templates, as well as the filter utilized during stimulation are shown. The performance in cardiac cycle identification and latency of the system are documented. To illustrate the general performance of the setup, its prediction accuracy and HRV influence were examined. Finally, there is a direct comparison between the two experimental setups BOSD and EBS.

3.1 Data Loss

For reliability in data retrieval, a recording of approximately 29 minutes was taken. The amount of data points per regular readout is 20. In some cases, 19, 21, and 22 were read out instead. This produced a CRC error in 1357 of 69487 (1.95%) data packages. The setup removed or replaced these data points to achieve a steady 20 samples. This way a total of 1894 data points were lost. The overall amount of data during the recording was 1.388.330 data points. Thus 0.1514% were lost.

3.2 Filter Application

In Figure 3.1 the comparison between the two further investigated filters can be seen. The same ECG was filtered with either lowpass. The filter with an order 140 with a 5Hz cutoff frequency leads to a broader & smaller QRS complex than the filter with an order 112 and cutoff at 6Hz.

The two filters were applied over approximately 10 minutes. The test run resulted in the histograms seen in Figure 3.2. Figure 3.2a shows the location of detected QRS complexes with a lowpass order of 140 and a cutoff frequency of 5Hz. 65.5% of detected QRS complexes are located at the correct position. The rest is located at the onset of the T wave. Figure 3.2b displays the lowpass with an order of 112 and a cutoff of 6Hz. The algorithm identified the QRS complex to 100% at the correct location. For the remaining project, the lowpass order 112 with a cutoff of 6Hz was utilized.

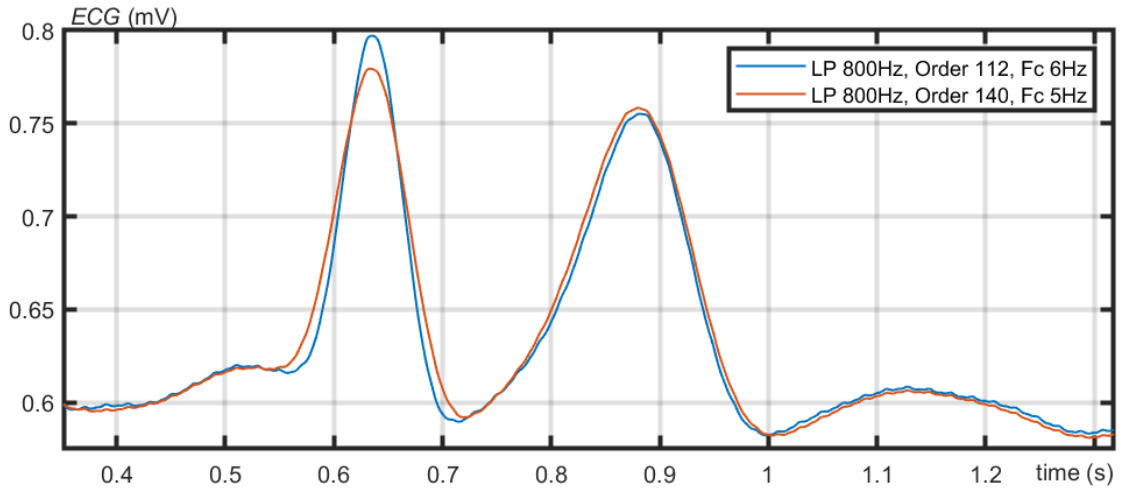

Figure 3.1: Two lowpass filters applied to an ECG cycle to illustrate their different effects on the QRS complex and T wave.

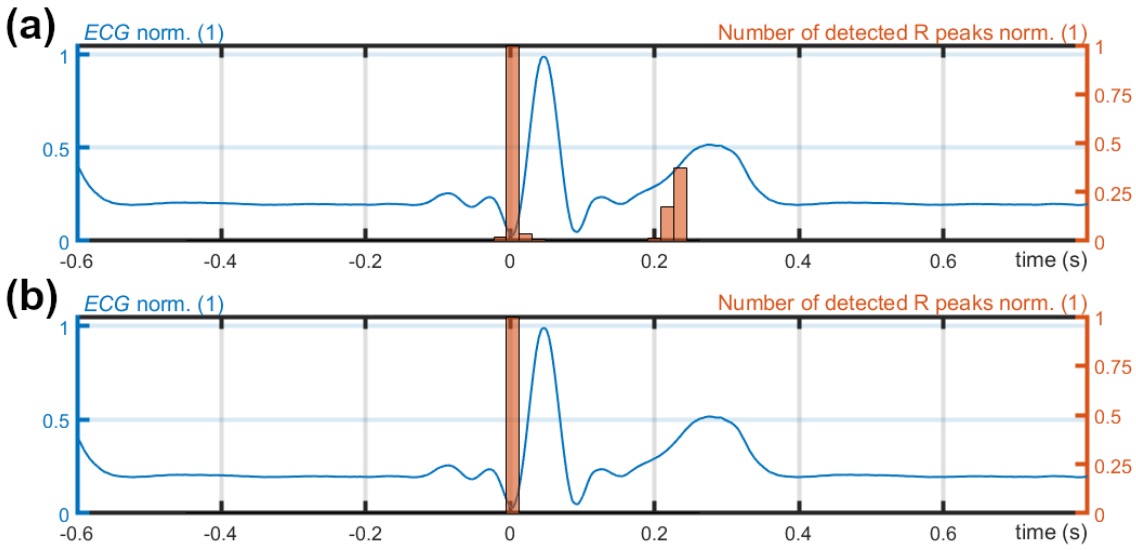

Figure 3.2: Histograms comparing two lowpass filters to determine the detection performance of the QRS complex. **(a)** The application of a lowpass of order 140 and a cutoff frequency of 5Hz. **(b)** This graph shows the lowpass of order 112 with a cutoff of 6Hz.

The designated filters for stimulation (lowpass) and pre/post-processing (bandpass) applied over a 4.5-second measurement can be seen in Figure 3.3 with the unfiltered raw signal in the background. When comparing the two filtered signals in the embedded window, it can be observed that the lowpass signal has only two waves remaining. Namely, the QRS complex and the T wave. The QRS complex retains a steeper slope compared to the T wave. The bandpass exhibits a more typical ECG signal. Its R peak is higher and the Q & S are more pronounced.

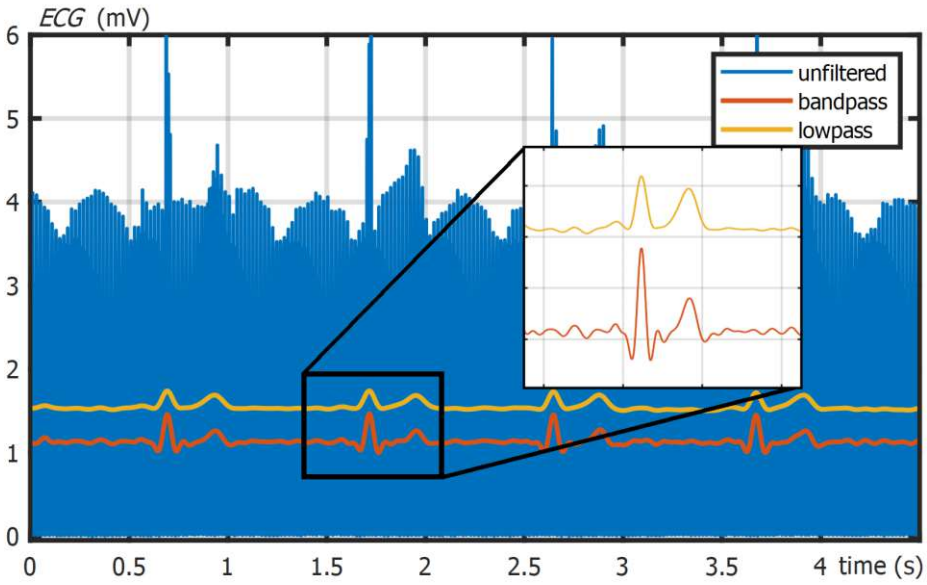

Figure 3.3: Visualization of the unfiltered ECG produced by the MAX86150 in blue. In the plot, as well as the embedded window, the signal can be seen filtered with a bandpass (red/orange) and a lowpass (yellow).

3.3 Cardiac Cycle Identification

To illustrate the effect of a preselection, a 60bpm ECG signal was recorded. The standard BOSD peak distance of 0.5 applied to the findpeaks function can be seen in Figure 3.4a. The distance approximated by the preselection method seen in 2.5 produced a mean peak distance of 1.07s. Rescaled to 80% the distance yielded 0.857 for application. Figure 3.4b shows the distance applied to the findpeaks function.

The standard distance detected 27 and the preselective distance 19 peaks. The total heartbeats depicted over the 20 seconds are 19.

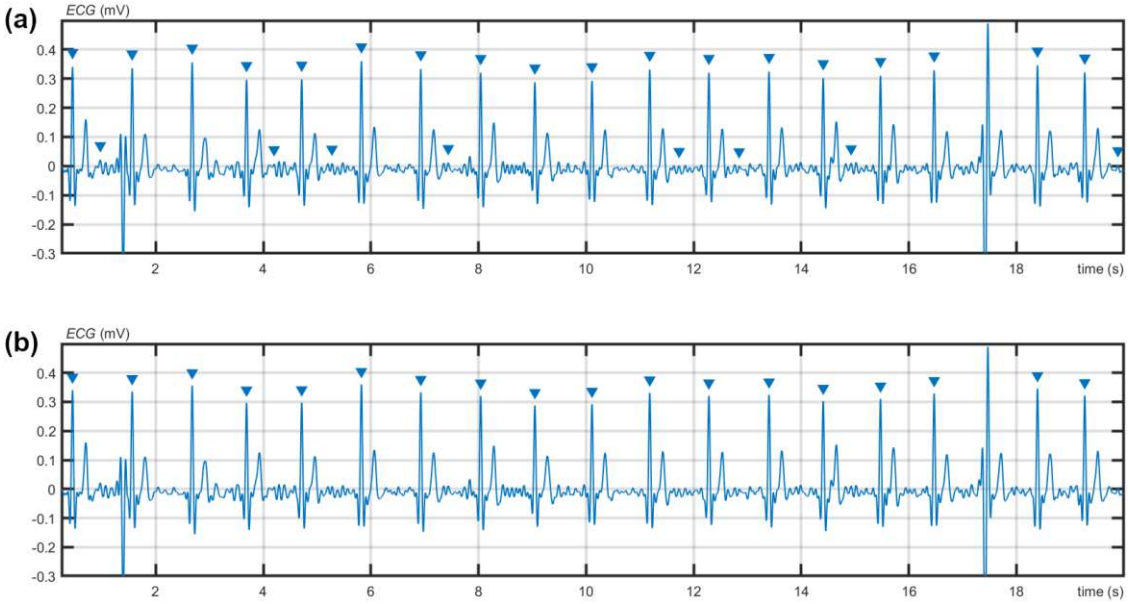

Figure 3.4: **(a)** A peak detection algorithm with a fixed minimum distance of 0.5s. **(b)** A variable minimum distance dependent on a preselection process applied to the peak detection algorithm.

3.4 Templates

In Figure 3.5 the ECG cycles for the template creation can be seen and in Figure 3.6 the resulting template through their cumulative median. In the 423 seconds, 418 heart cycles were detected. Of these cycles, 6 were disqualified. The displayed cutoff is 400ms after the Q peak.

Figure 3.8 shows the PPG template, created from a 396s recording (as seen in Figure 3.7). 366 heart cycles were identified and 16 were disqualified. The displayed cutoff is set with the onset of the next heart cycle.

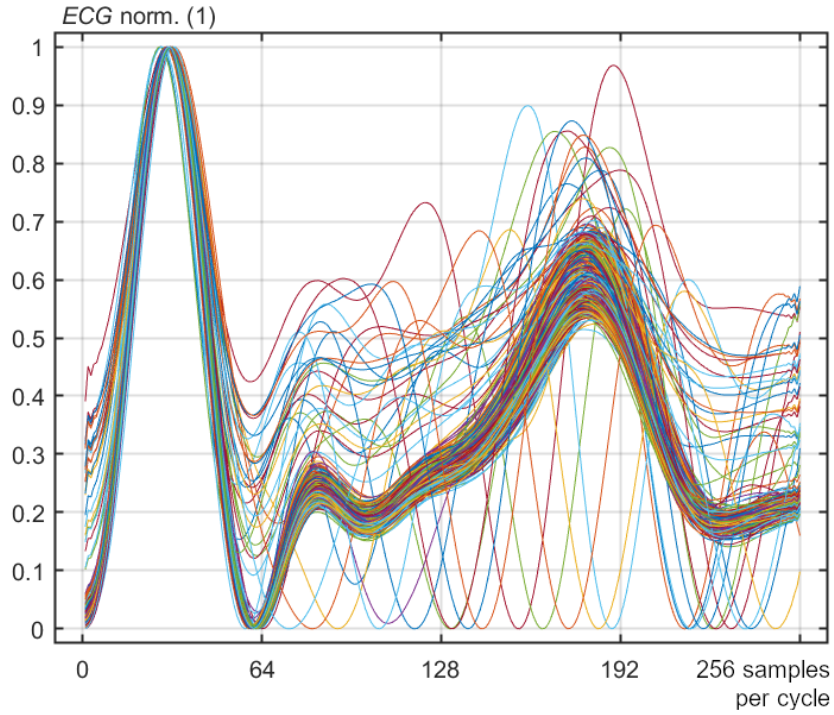

Figure 3.5: Collective ECG cycles of 423s with 412 heart cycles normalized to a common scale. The participant was sitting and at rest.

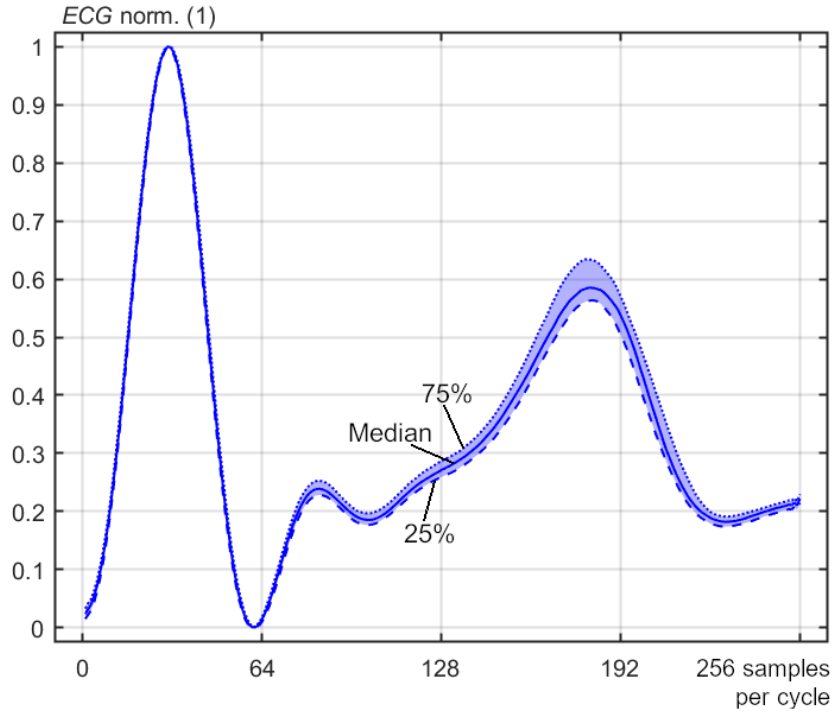

Figure 3.6: The median and interquartile range of 412 ECG heart cycles, recorded with MAX86150.

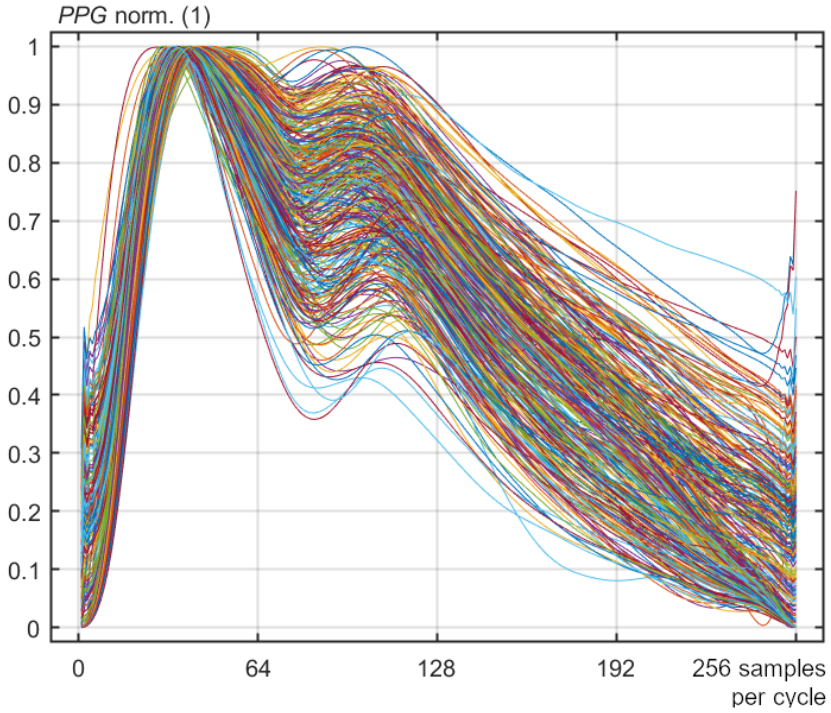

Figure 3.7: Collective PPG cycles of 396s with 366 heart cycles normalized to a common scale. The participant was sitting and at rest.

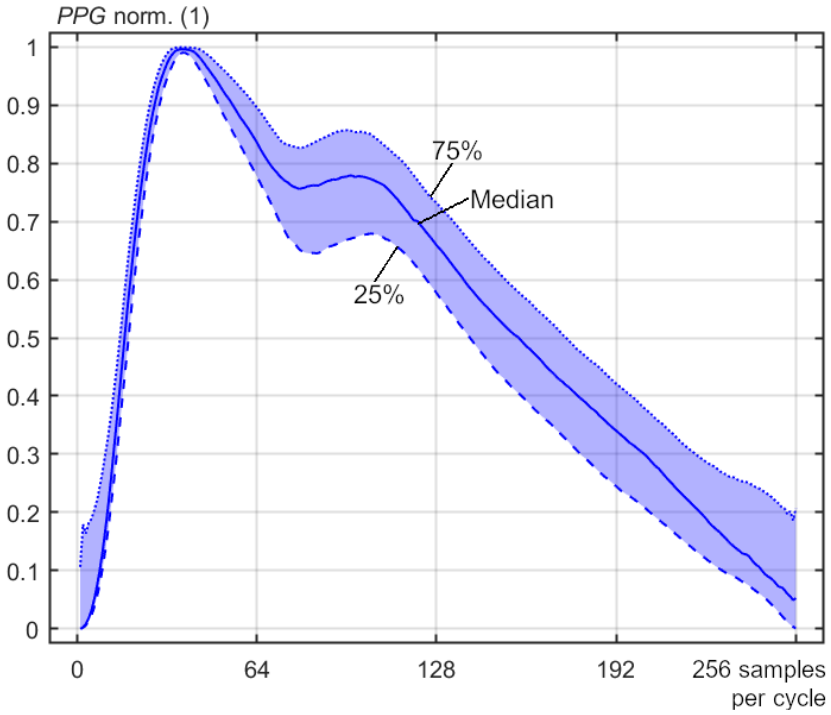

Figure 3.8: The median and interquartile range of 364 PPG heart cycles, recorded with MAX86150.

The first 15 cross-correlation coefficients of 4 different ECG calibration runs can be seen in Table 3.1. They show whether a recorded ECG section had enough correlation with the template created above. The template was tested with two different cutoffs at 400ms after the R peak and with the Q peak of the next cardiac cycle. For the test, a 60bpm and 100bpm signal were applied. These test recordings are illustrated in Figure 3.9 via their median, 1st, and 3rd quantile. The previously created template is depicted in red. The graphs are depicted in the same order in Figure 3.9**a-d** as the table from the left to the right.

In total in the test runs of

- Figure 3.9**a**, 60bpm & 400ms, 18/18 pass.
- Figure 3.9**b**, 100bpm & 400ms, 33/33 pass.
- Figure 3.9**c**, 60bpm & Q peak, 18/18 pass.
- Figure 3.9**d**, 100bpm & Q peak, 0/33 pass.

Table 3.1: Cross-correlation calculation between the first 15 ECG cycles at frequencies of 60bpm & 100bpm and the template. A fixed starting point was set at the Q peak and cutoffs were set at the next Q peak & 400ms after the R peak. Correlation coefficients higher than 0.65 were accepted as True, while lower were identified as False.

60bpm, 400ms		**100bpm, 400ms**		**60bpm, Q peak**		**100bpm, Q peak**	
Coeff.	**>0.65**	**Coeff.**	**>0.65**	**Coeff.**	**>0.65**	**Coeff.**	**>0.65**
0.98	1	0.87	1	0.66	1	-0.040	0
0.99	1	0.91	1	0.93	1	0.040	0
0.99	1	0.92	1	0.98	1	-0.090	0
0.99	1	0.90	1	0.98	1	0.020	0
0.99	1	0.94	1	0.94	1	0.050	0
0.99	1	0.89	1	0.95	1	0.040	0
0.99	1	0.92	1	0.91	1	-0.020	0
0.99	1	0.85	1	0.97	1	0.080	0
0.99	1	0.91	1	0.96	1	0.030	0
0.99	1	0.89	1	0.96	1	0.030	0
0.99	1	0.90	1	0.95	1	-0.020	0
0.97	1	0.90	1	0.95	1	0.030	0
0.99	1	0.85	1	0.98	1	0.16	0
0.98	1	0.86	1	0.95	1	0.080	0
0.98	1	0.89	1	0.97	1	0.070	0

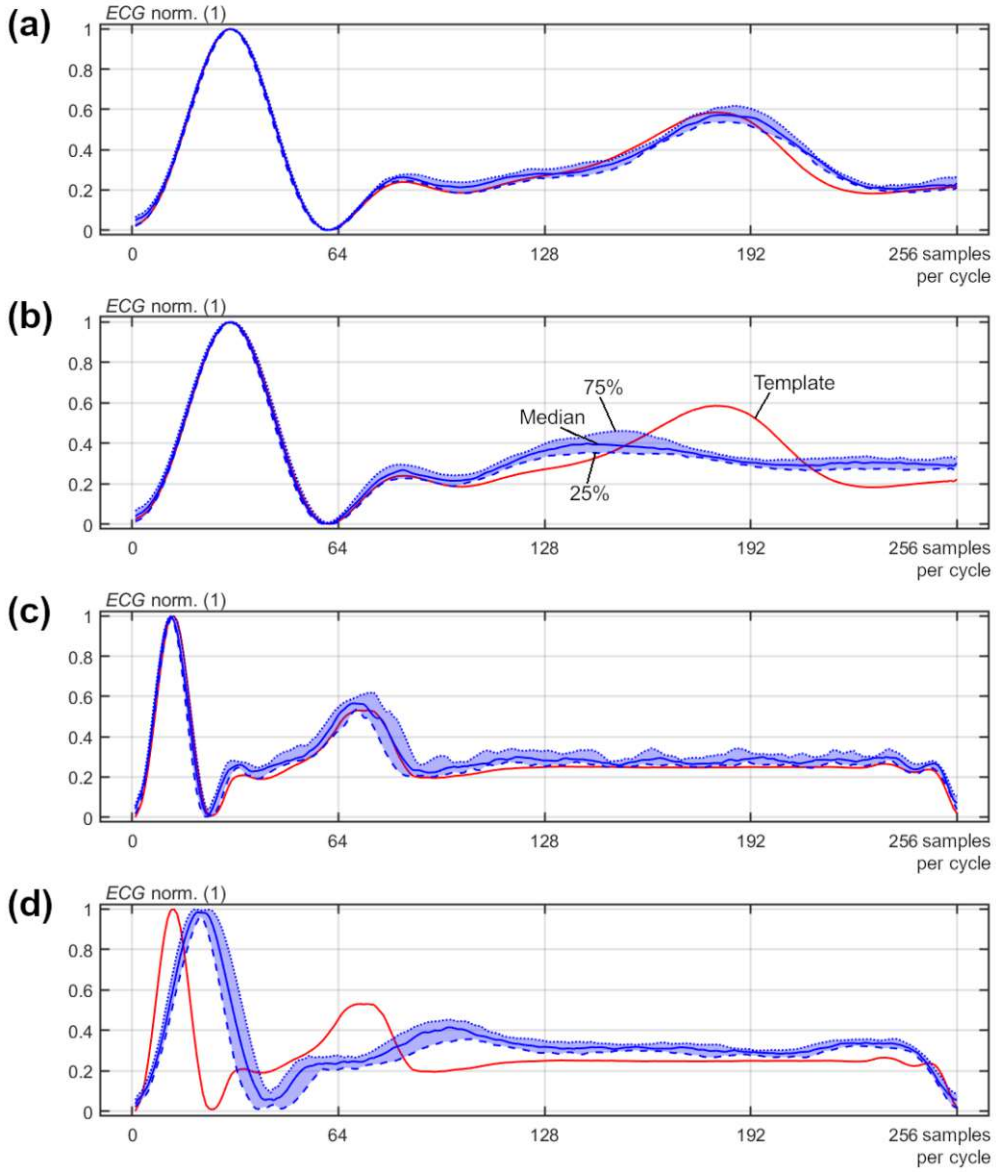

Figure 3.9: ECGs recorded over different bpm and normalized to 256 from a fixed starting point & variable cutoff in blue. Additionally, an adjusted ECG template is depicted with the same extraction parameters and 60bpm recording frequency in red. **(a)**, **(b)** The ECG has a cutoff of 400ms after the R peak. Figure **(a)** shows 60bpm and **(b)** 100bpm. **(c)**, **(d)** They show a signal with a cutoff at the next Q peak. The recording frequencies were **(c)** 60bpm and **(d)** 100bpm.

The first 15 cross-correlation coefficients of 4 different PPG calibration runs can be seen in Table 3.2. They show whether a recorded PPG section had enough correlation with the template created above. The template was tested with two different cutoffs at 400ms after the systolic peak and at the beginning of the next cardiac cycle. For the test, a 60bpm and 100bpm signal were applied. These test recordings are illustrated in Figure 3.10 via their median, 1st, and 3rd quantile as well as the template in red. The graphs are shown in the same order from Figure 3.10**a - d** as the table from the left to the right.

In total in the test runs of

- Figure 3.9**a**, 60bpm & 400ms, 18/18 pass.
- Figure 3.9**b**, 100bpm & 400ms, 29/35 pass.
- Figure 3.9**c**, 60bpm & Q peak, 18/18 pass.
- Figure 3.9**d**, 100bpm & Q peak, 11/35 pass.

Table 3.2: Cross-correlation calculation between the first 15 PPG cycles at frequencies of 60bpm & 100bpm and the Template. A fixed starting point was set at the heart cycle onset and cutoffs were set at the next cycle onset & 400ms after the systolic peak. Correlation coefficients higher than 0.65 were True, while lower were identified as False.

60bpm, 400ms		**100bpm, 400ms**		**60bpm, Onset**		**100bpm, Onset**	
Coeff.	**>0.65**	**Coeff.**	**>0.65**	**Coeff.**	**>0.65**	**Coeff.**	**>0.65**
0.98	1	0.84	1	0.95	1	0.22	0
0.97	1	0.54	0	0.96	1	0.61	0
0.98	1	0.92	1	0.98	1	0.24	0
0.97	1	0.85	1	0.99	1	0.53	0
0.95	1	0.78	1	0.96	1	0.23	0
0.93	1	0.59	0	0.96	1	0.43	0
0.97	1	0.77	1	0.94	1	0.67	1
0.94	1	0.78	1	0.97	1	0.76	1
0.95	1	0.96	1	0.99	1	0.52	0
1	1	0.78	1	0.97	1	0	0
0.87	1	0.75	1	0.94	1	0.25	0
1	1	0.75	1	0.95	1	0.61	0
0.95	1	0.74	1	0.94	1	0.39	0
0.93	1	0.81	1	0.98	1	0.81	1
0.96	1	0.62	0	0.99	1	0.27	0

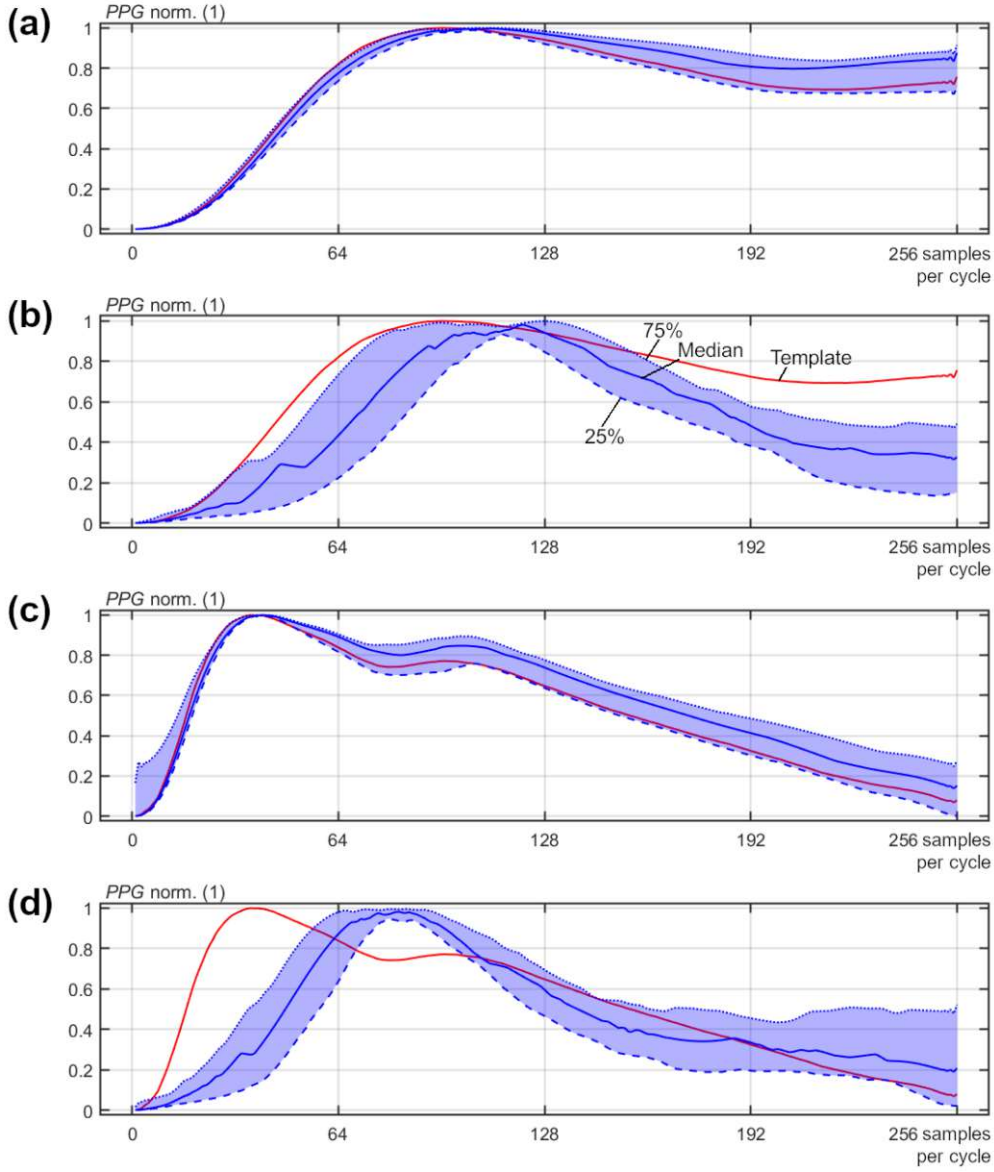

Figure 3.10: PPGs recorded over different bpm and normalized to 256 from a fixed starting point & variable cutoff in blue. Additionally, an adjusted PPG template is depicted with the same extraction parameters and 60bpm recording frequency in red. **(a)**, **(b)** The PPG has a cutoff of 400ms after the systolic peak. Figure **(a)** shows 60bpm and **(b)** 100bpm. **(c)**, **(d)** They show a signal with a cutoff at the onset of the heart cycle. The recording frequencies were **(c)** 60bpm and **(d)** 100bpm.

3.5 Latency

To identify the latency, the EBS setup was run four times. Each measurement was newly calibrated. The time taken sums up to approximately 30 minutes. Its breakdown can be seen in Table 3.3. All stimulation onsets further than 200ms away from the detected QR slope were considered a False Positive (FP), the rest a True Positive (TP). Of the ECG cycles during these iterations, 86.6% were detected. Of these detected peaks, 3.2% were miss identified slopes, the rest were true QRS complexes.

Table 3.3: ECG measurements to evaluate the latency are depicted. The detected QRS complexes of the ECG are detailed and split up into correctly/incorrecly identified cardiac cycles.

Measurement	time (s)	Peaks	Detected	TP	FP
1	490	500	480	468	12
2	352	365	314	302	12
3	357	367	303	299	4
4	686	596	486	466	22
Total:	1885	1828	1583	1535	50

The time difference between stimulation onset and the detected QR interval can be seen in Figure 3.11. Two distributions are displayed. The first one being the correctly identified TP, listed in Table 3.3 above. The second one is FP data. The FP data originates partially from the T wave where the slope was above the threshold.

The mean value of the TP distribution is 96 milliseconds. Its empirical standard deviation is ±27.1ms.

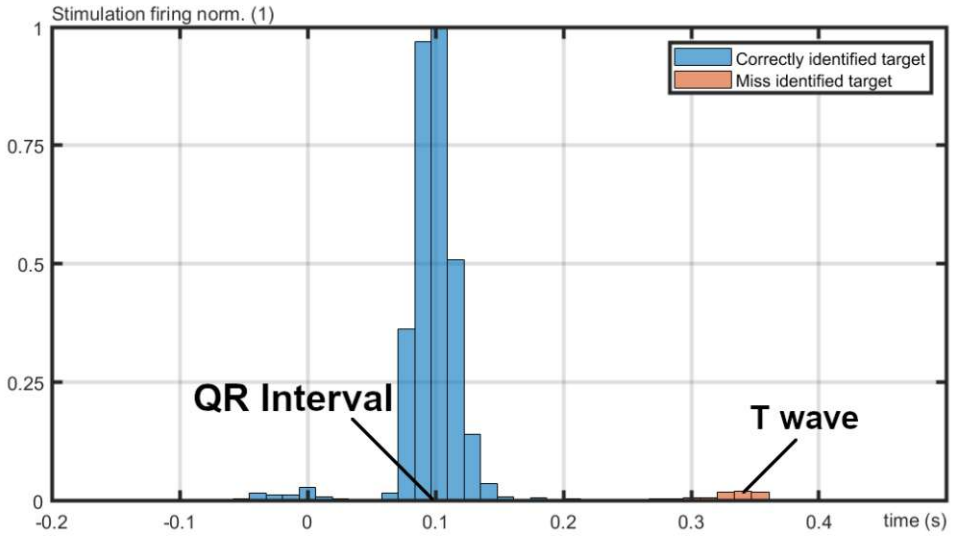

Figure 3.11: The distribution shows the stimulation latency of the EBS setup. The targeted Q peak can be seen at 96ms. In some cases the T wave was miss identified and stimulated.

3.6 Detection Precision

The accuracy in R peak detection is detailed in Table 3.4. The distributions of step size 50ms & 25ms for the 50ms window are listed. The time difference represents the deviation from the R peak in milliseconds. These differences are in 1.25ms steps, the maximum resolution for an 800Hz sampling frequency.

For the 50ms steps, a total of 601s were recorded. During this time 631 heartbeats occurred, of which 506 were identified. Out of those detected, 7 were disqualified. The rest was spread from -1.25ms to 15ms as documented by the table. The standard deviation of the stimulation around the target location is ±84.2ms.

For the 25ms steps a total of 603s were recorded, 593 heartbeats occurred, 592 were detected and none disqualified. As can be seen in the table, the spread is tighter and restricted from -1.25ms to 2.5ms. The standard deviation for the target location is ±67ms.

Table 3.4: The distributions of 25ms and 50ms steps for a 50ms time window to identify the QRS complex of an ECG.

Time Difference (ms)

	-1.25	**0**	**1.25**	**2.50**	**3.75**	**5.00**	**6.25**
50ms	16	185	153	20	17	12	18
25ms	42	299	249	2	0	0	0

	7.50	**8.75**	**10.00**	**11.25**	**12.50**	**13.75**	**15.00**
50ms	13	15	9	14	12	9	6
25ms	0	0	0	0	0	0	0

3.7 Setup Evaluation

Two measurements were made, one with the setup shown in Figure 2.8, Section 2.4 for the evaluation of predicted vs actual stimulation timepoint. Additionally, the measurement was investigated for the HRV influence & stimulation precision. The second measurement was a parallel setup application for a performance review between BOSD & EBS, seen in Figure 2.11, Section 2.6.3.

3.7.1 Stimulation Accuracy

The recording time was 22 minutes and 37 seconds. The stimulation pulse rising edge timepoints subtracted from their corresponding R peaks are shown. This was done for both the timepoint of the outgoing stimulation command in Simulink, as well as BIOPAC receiving the stimulation pulse.

The respective distributions can be seen superimposed on each other in Figure 3.12. Orange shows the location Simulink predicts the stimulation onset to be (through its command). The blue distribution represents the detected stimulation beginning in BIOPAC. The mean of Simulink is -129.4ms with an std of ±66.7ms. For BIOPAC the mean is -134.3ms and its std is ±67.9ms.

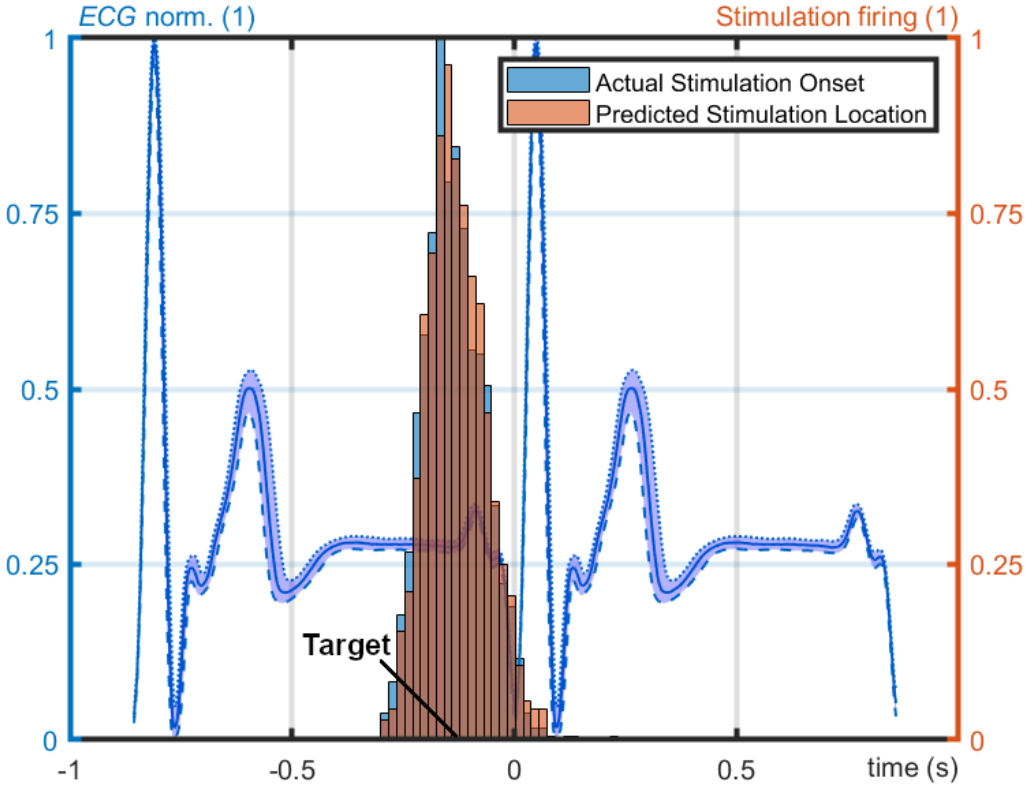

Figure 3.12: Recorded distributions of stimulation pulse onset positions aiming at the Target point. One recording shows the predicted stimulation location by Simulink. The other distribution is the stimulation onset measured by the BIOPAC System.

3.7.2 HRV Influence

The same measurement as in Section 3.7.1 is used for this evaluation. The difference between the stimulation onset and the R peak from which Simulink predicted are shown in Figure 3.13a. Figure 3.13b shows the HRV by SDNN for each detected/stimulated heart cycle.

The stimulation standard deviation was ±13.3ms. The mean heart rate over the recording was 870.5ms with an std of ±87ms.

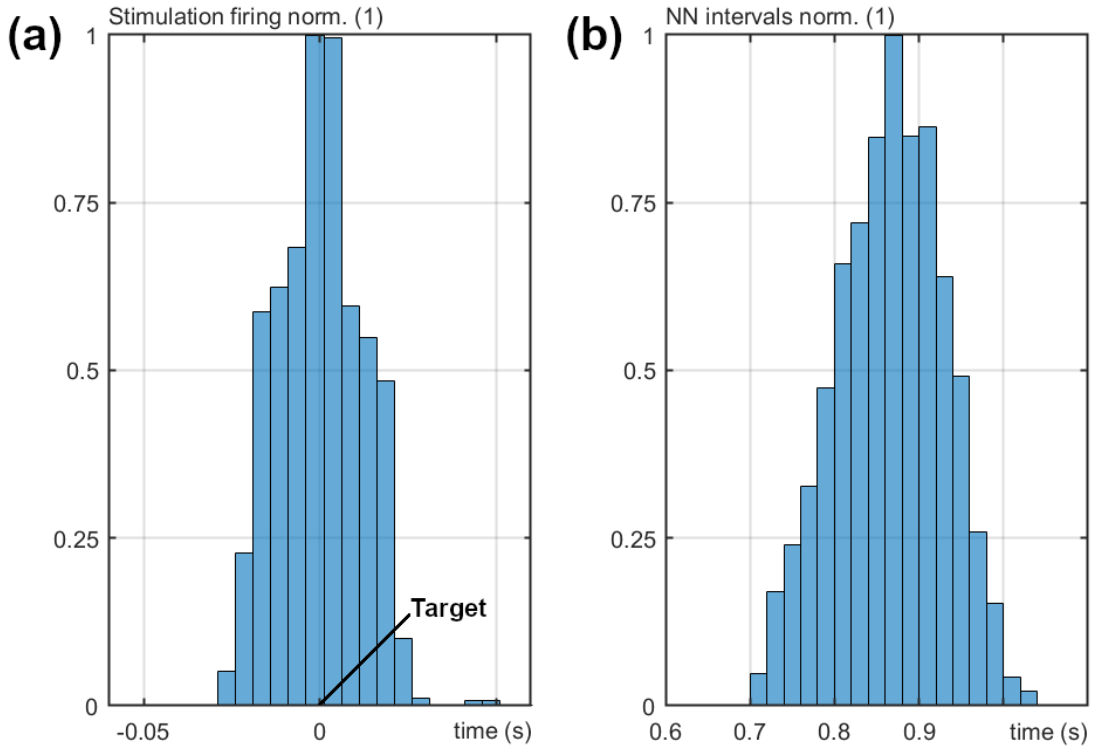

Figure 3.13: **(a)** This graph shows the precision in hitting the stationary target point in the EBS. **(b)** This figure depicts the HRV of the participant for all stimulated ECG heart cycles.

3.7.3 Performance Comparison

In Figure 3.14 the result of running both setups simultaneously can be seen over a time of 10 minutes. Figure 3.14a depicts the implementation of the MAX86150 sensor, while Figure 3.14b shows the BOSD setup with BIOPAC.

The EBS setup had a standard deviation of ±67.2ms around the target point (Q peak), with a total of 695 heart cycles detected out of 699. In comparison, the BIOPAC setup detected a total of 563 QR complexes out of 699 with a standard deviation of ±67.1ms.

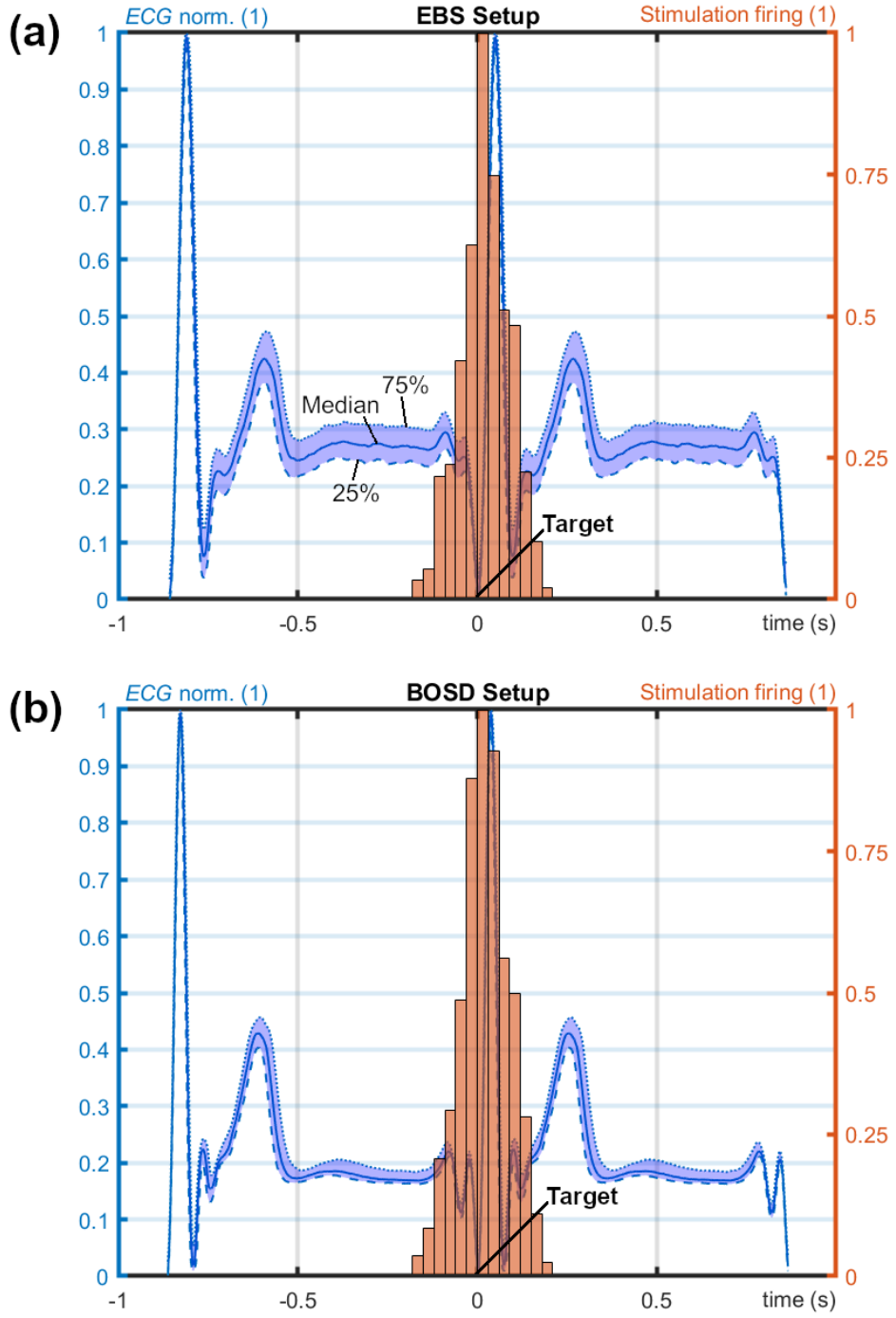

Figure 3.14: Synchronized stimulation setups aiming at the Q peak with ECG as a feedback and their distributions over a 10 minute recording. **(a)** The distribution of the EBS with the MAX86150 sensor as a feedback device. **(b)** The distribution of the BOSD, featuring the BIOPAC System as a feedback device.

4 Discussion

The purpose of this thesis was to evaluate the integrated sensor MAX86150 as a replacement for the BIOPAC System as a biofeedback source for the aVNS setup and improve the system in general. To implement the sensor it had to be set up with a suitable sampling frequency and reliable communication to the established system. Furthermore, new templates for the calibration were created as well as procedures for improved signal detection. The hardware delay was identified, the stimulation precision evaluated and the influence of the HRV investigated. To make the EBS setup comparable to the BOSD, a simultaneous synchronized test run was conducted.

4.1 Experimental Setup

The MAX sensor is an integrated sensor providing a high range of sampling frequency while measuring ECG and PPG in sync. It can be brought into a standby mode, reducing energy consumption to 0.7μA to save energy. These circumstances make it an ideal sensor module for portable battery-powered applications [37]. The configuration parameters were mainly chosen due to the recommendations made by Maxim Integrated. The document suggests setting up 2 LEDs and the ECG [38]. When maintaining the recommended pulse width length for LEDs, the maximum sampling frequency with 2 LEDs is restricted to 400Hz. We decided one LED is sufficient for the purpose of the experimental setup. Through the reduction, the frequency could be doubled, providing us with 800Hz of PPG & ECG. The frequency could be increased further by deviating from the recommended pulse width length [37].

The data transmission between the MAX sensor, the MCU and Simulink shows a reliable transfer of the data points. The CRC does flag 1.95% as erroneous, but on further investigation, it does not originate in the data transfer. Instead, the MCU sometimes extracts the data too early or too late. This results in a CRC value calculated out of e.g. 21 data points on the MCU side, whereas the Simulink side expects and uses a fixed 20 frame for CRC calculation. Thus, the mismatch and raised error. Currently, those errors and the data point surplus are ignored. A shortage is compensated by duplicating the data point of the previous package at this position. By preserving the other data points, the loss in data is reduced to 0.1513%. In other words, one data point every ~660 data points is lost. Furthermore, the EBS setup utilizes windows of 50ms for linear interpolation, minimizing the impact of a 1.25ms to 3.75ms loss further.

4.2 Filter Design

The filter design had to fulfill some benchmarks to enable utilization for the EBS setup.

- QRS complex and T wave need to differ in their slope.
- Filter order had to be kept low.
- The baseline should exhibit a low gradient.

It is evident in Figure 3.1 and Figure 3.2 that a change to an order too high or a cutoff frequency too low can impact the ECG filtering to a point where the QRS complex and T wave look very similar. This has as result that the threshold for the QR slope detection can allow for steep T waves to be miss identified. For the lowpass filter with an order of 140 and a cutoff frequency of 5Hz, as seen in the upper Figure 3.2, this was the case with a third of the identifications located at the T wave. It is to be noted, that these were consecutive measurements and the repeated calibration has an influence on the proper identification. Furthermore, baseline wander might inhibit the detection of QRS complexes in downturns and the other way around, promote miss identification during upturns.

The filter order directly influences the time delay of the signal. This setup predicts the next heartbeat and can therefore not surpass this time limit. The approximate maximum bpm for young individuals is 220 [32]. As an approximation, a maximum heart rate of 200bpm was considered, providing a maximum latency of 500ms. The chosen stimulation lowpass filter takes up a time of 70ms.

The additional filter for pre- and postprocessing purposes for the ECG is utilized to detect the QRS complex more readily. It provides a higher R peak and deeper Q & S peaks, as seen in Figure 3.3. This facilitates the cardiac cycle extraction and correct QRS identification for the QR slope calibration of the stimulation filter.

4.3 Cardiac Cycle Identification

As seen in Figure 3.4a, the findpeaks function identifies 8 additional peaks. Those are then examined in the cross-correlation process and rejected, providing the user with the prompt to recalibrate. If the calibration process does accept the 20s recording, it will take the slope of every identified peak. Even the ones denied during the cross-correlation. Thus, the threshold is distorted. To solve this problem in identification, the preselection process was created to ensure a correct detection as seen in Figure 3.4b. The mean peak distance is rescaled to 0.8 to compensate for marking inaccuracy and the eventuality of a higher frequency being present. Miss identification can still happen and influence the threshold calculation, but it is reduced considerably.

The template creation for cross-correlation validation provided a challenge in choosing a proper cutoff. The BOSD setup chose to cut off the ECG and PPG at the onset of the following cycle (Q peak or rising edge of the systolic peak). This works for heart rates

similar enough to the template as seen in Figure 3.9c and Figure 3.10c. But as seen in Figure 3.9d and Figure 3.10d, as well as in Tables 3.1 & 3.2, the calibration can fail for heart rates with a high difference between measurement and template. This led to cross-correlation analysis denying the calibration for the correct biosignals. By choosing a point of interest and adding 400ms to it, the distances stay similar for different bpm. This can be seen in Figure 3.9ab and Figure 3.10cd, as well as in the Tables 3.1 & 3.2. Furthermore, the biosignal varies more towards the end when normalizing it, as seen in Figure 3.5 and Figure 3.7. Therefore, a cutoff after 400ms removes some of the variable area. For the ECG, the 400ms were chosen because the T wave is at maximum 300ms away from the QRS complex [32]. The PPG cutoff was inspired by the ECG cutoff.

4.4 Setup Evaluation

By setting $\triangle t_{\text{Delay}} = 0$ for the latency detection, the setup stimulates as soon as it sees the QR slope. The difference in stimulation onset and ECG QR complex resulted in the hardware delay. The experimental setup sometimes misidentified signal sections as a QR slope and stimulated them. This necessitated an identification of correctly detected QR slopes. To ensure detection of the new latency, the cutoff was taken as approximately double the latency of the BOSD setup (85ms). Stimulation onsets further than 200ms away from the R peak were removed. The latency increased to 96ms $\pm$27.1ms standard deviation, compared to the BOSD setup with 85ms. Considering the stimulation takes place at the predicted next heart cycle with a hypothetical maximum of 200 bpm, the 96ms fall far below the 500ms limit.

For the detection precision, the reduction in step time from 50ms to 25ms for QR slope and R peak detection restricted the deviation from 15ms to 2.5, as seen in Table 3.4. The increased precision in detection provides the possibility of a better prediction for the next heart cycle. Moreover, the QRS complex identification performed better with 25ms steps. For the 50ms steps, only 80% were detected, while the 25ms steps found nearly 100%. It is stated in the paper by Dabiri et al. [36], that the BOSD setup identified >90% of the peaks. The reduced step size setup in the EBS surpasses this. Due to the fact that the recordings were made in succession, it is to be considered that the calibration and biosignals produced by the participant can vary and influence the results.

The in Figure 3.12 depicted stimulation accuracy of Simulink was investigated to determine whether it predicts the stimulation pulse at the correct position after the latency implementation. Furthermore, it was analyzed if there are differences between the distribution shown in Simulink and the actual stimulation on site. The distributions produced by Simulink and BIOPAC in Figure 3.12 are at the same position, with a difference in mean of 5.1ms. The standard deviation difference lies at 1.2ms. It can be assumed, that the latency was adjusted correctly.

In Figure 3.13a, the deviation around the fixed timepoint of stimulation can be seen. This point is defined during calibration and determines the time taken after an identified R peak to wait until stimulation. Its standard deviation shows the sole precision of the hardware at ±13.3ms. This precision range originates from the 25ms data package size. It is the bottleneck of the system. In Figure 3.13b the HRV is seen, acquired through SDNN. The stimulation timepoint is fixed to a distance after the detected R peak, but the target point of the cardiac cycle is HRV dependent. Therefore, the proximity between stimulation onset and target point varies due to the HRV. This leads to a lower stimulation precision in regard to the cardiac cycle, as seen in Figure 3.14a.

The comparison between the BOSD setup and the EBS setup shows little difference in their stimulation distribution around the point of interest. In Figure 3.14 a direct comparison can be seen. Figure 3.14a shows the EBS setup with the MAX sensor, whereas Figure 3.14b shows the BOSD setup. Their standard deviations are ±67.2ms by the EBS and ±67.1ms by the BOSD setup. The EBS setup was able to identify 132 peaks more out of a total of 699 ECG cycles than the BOSD.

5 Conclusion

All in all the MAX86150 sensor seems to be a good replacement for the BIOPAC System of the TU Wien aVNS setup. Due to the replacement, the experimental setup is now portable and capable of relying on a battery. It provides a steady supply of data points for ECG and PPG. Some data loss does occur, but it is negligible. The sampling frequency is increased from 500Hz to 800Hz while providing PPG & ECG simultaneously and in synchronization to Simulink. The maximum precision of the hardware is at an std of $\pm$13.3ms. This originates in the sampling frequency at 800Hz, delivering data points every 25ms. It is the current bottleneck of the experimental setup. Due to the HRV dependent target point in the cardiac cycle, the overall stimulation precision is decreased to $\pm$67.2ms. Concerning the stimulation performance, the EBS is as good as the BOSD setup in stimulation precision and identified approximately 19% more heart cycles in the performed measurement.

The closed-loop aVNS approach may serve as an alternative to the classical VNS approach, activating the Vagus Nerve to the same level. Instead of implanting a VNS device in the neck region, the aVNS setup relies on surface or needle electrodes for stimulation at the ear. For this reason, aVNS is a non-invasive or minimally invasive treatment. Through the closed-loop approach enabled by the biofeedback, the aVNS can adjust its stimulation to correct, for instance, under- or over-stimulation. Furthermore, the stimulation can be applied in synchronization with cardiac events or other body rhythms. In general, VNS is a promising approach for treatment of, among others, refractory epilepsy, inflammation, psychiatric disorders, pain and atrial fibrillation. Therefore, electroceuticals, like closed-loop aVNS, could be a viable substitute to drugs in the future.

6 Outlook

The data point extraction could be improved by replacing the interrupt timer for data requesting on the MCU side with an interrupt by the sensor side. This would provide more stability to the system. By adjusting the cardiac cycle identification and extraction in the calibration process, cycle miss identification could be prevented. Furthermore, predictive measures to compensate for the HRV could be implemented. Either by utilizing the underlying respiration sine in ECG or through predictive measures based on the past cardiac cycle distances. This could close the gap between the stimulation precision at ± 67.2ms and the maximum hardware precision at ± 13.3. The setup needs to be optimized for long-term usage. The current calibration process provides momentary parameters that become invalid after some time. Furthermore, motion artifacts could be taken into consideration in the future.

Appendix

Table 6.1: System Control (0x0D)

BIT	7	6	5	4	3	2	1	0
Field	—	—	—	—	—	FIFO_EN	SHDN	RESET
Reset	—	—	—	—	—	0x0	0x0	0x0
Access Type	—	—	-	—	—	Write, Read	Write, Read	Write, Read

Table 6.2: FIFO Configuration (0x08)

BIT	7	6	5	4	3	2	1	0
Field	—	A_FULL_ CLR	A_FULL_ TYPE	FIFO_ ROLLS_ ON_FULL	FIFO_A_FULL[3:0]			
Reset	—	0x0	0x0	0x0	0xF			
Access Type	—	Write, Read	Write, Read	Write, Read	Write, Read			

Table 6.3: FIFO Data Control Register 1 (0x09)

BIT	7	6	5	4	3	2	1	0
Field	FD2[3:0]				FD1[3:0]			
Reset	0x0				0x0			
Access Type	Write, Read				Write, Read			

Table 6.4: LED2 PA (0x12)

BIT	7	6	5	4	3	2	1	0
Field	LED2_PA[7:0]							
Reset	0x00							
Access Type	Write, Read							

Table 6.5: PPG Configuration 1 (0x0E)

BIT	7	6	5	4	3	2	1	0
Field	PPG_ADC_RGE[1:0]		PPG_SR[3:0]				PPG_LED_PW[1:0]	
Reset	0x0		0x0				0x0	
Access Type	Write, Read		Write, Read				Write, Read	

Table 6.6: PPG Configuration 2 (0x0F)

BIT	7	6	5	4	3	2	1	0
Field	—	—	—	—	—	SMP_AVE[2:0]		
Reset	—	—	—	—	—	0x0		
Access Type	—	—	—	—	—	Write, Read		

Table 6.7: ECG Configuration 1 (0x3C)

BIT	7	6	5	4	3	2	1	0
Field	—	—	—	—	—	ECG_ADC_CLK	ECG_ADC_OSR[1:0]	
Reset	—	—	—	—	—	0x0	0x0	
Access Type	—	—	—	—	—	Write, Read	Write, Read	

Table 6.8: ECG Configuration 3 (0x3E)

BIT	7	6	5	4	3	2	1	0
Field	—	—	—	—	PGA_ECG_GAIN[1:0]		IA_GAIN[1:0]	
Reset	—	—	—	—	0x0		0x2	
Access Type	—	—	—	—	Write, Read		Write, Read	

Table 6.9: FIFO Write Pointer (0x04)

BIT	7	6	5	4	3	2	1	0
Field	—	—	—	FIFO_WR_PTR[4:0]				
Reset	—	—	—	0x00				
Access Type	—	—	—	Write, Read				

Table 6.10: Overflow Counter (0x05)

BIT	7	6	5	4	3	2	1	0
Field	—	—	—	OVF_COUNTER[4:0]				
Reset	—	—	—	0x00				
Access Type	—	—	—	Read Only				

Table 6.11: FIFO Read Pointer (0x06)

BIT	7	6	5	4	3	2	1	0
Field	—	—	—	FIFO_RD_PTR[4:0]				
Reset	—	—	—	0x00				
Access Type	—	—	—	Write, Read				

Table 6.12: FIFO Data Register (0x07)

BIT	7	6	5	4	3	2	1	0
Field	FIFO_DATA[7:0]							
Reset	0x00							
Access Type	Write, Read							

List of Figures

List of Tables

Bibliography

[1] S. Mishra, "Electroceuticals in medicine – the brave new future", *Indian Heart Journal*, vol. 69, no. 5, pp. 685–686, 2017, ISSN: 0019-4832. DOI: https://doi.org/10.1016/j.ihj.2017.10.001. [Online]. Available: https://www.sciencedirect.com/science/article/pii/S0019483217308131.

[2] C. L. LYNCH and M. R. POPOVIC, "Functional electrical stimulation", *IEEE Control Systems Magazine*, vol. 28, no. 2, pp. 40–50, 2008. DOI: 10.1109/MCS.2007.914689.

[3] K. Famm, B. Litt, K. J. Tracey, E. S. Boyden, and M. Slaoui, "A jump-start for electroceuticals", *Nature*, vol. 496, no. 7444, pp. 159–161, Apr. 2013.

[4] M. Trepel, *Neuroanatomie: Struktur und Funktion*. Elsevier Health Sciences, 2012.

[5] J. Tindle and P. Tadi, "Neuroanatomy, parasympathetic nervous system", en, in *StatPearls*, Treasure Island (FL): StatPearls Publishing, Jan. 2022.

[6] H.-R. Berthoud and W. Neuhuber, "Functional anatomy of afferent vagal system", *Autonomic neuroscience : basic & clinical*, vol. 85, pp. 1–17, Jan. 2001. DOI: 10.1016/S1566-0702(00)00215-0.

[7] J. A. Clancy, S. A. Deuchars, and J. Deuchars, "The wonders of the wanderer", en, *Exp Physiol*, vol. 98, no. 1, pp. 38–45, Jul. 2012.

[8] S. Breit, A. Kupferberg, G. Rogler, and G. Hasler, "Vagus nerve as modulator of the brain–gut axis in psychiatric and inflammatory disorders", *Frontiers in Psychiatry*, vol. 9, 2018, ISSN: 1664-0640. DOI: 10.3389/fpsyt.2018.00044. [Online]. Available: https://www.frontiersin.org/article/10.3389/fpsyt.2018.00044.

[9] E. Ben-Menachem, R. Mañon-Espaillat, R. Ristanovic, *et al.*, "Vagus nerve stimulation for treatment of partial seizures: 1. a controlled study of effect on seizures", *Epilepsia*, vol. 35, no. 3, pp. 616–626, 1994. DOI: https://doi.org/10.1111/j.1528-1157.1994.tb02482.x. eprint: https://onlinelibrary.wiley.com/doi/pdf/10.1111/j.1528-1157.1994.tb02482.x. [Online]. Available: https://onlinelibrary.wiley.com/doi/abs/10.1111/j.1528-1157.1994.tb02482.x.

[10] D. E. Connor Jr, M. Nixon, A. Nanda, and B. Guthikonda, "Vagal nerve stimulation for the treatment of medically refractory epilepsy: A review of the current literature", en, *Neurosurg Focus*, vol. 32, no. 3, E12, Mar. 2012.

[11] C. W. Wright, L. Bu, A. Jones, and N. Calder Green, "Vns therapy for the treatment of epilepsy", in *Electroceuticals: Advances in Electrostimulation Therapies*, A. Majid, Ed. Cham: Springer International Publishing, 2017, pp. 181–204, ISBN: 978-3-319-28612-9. DOI: 10.1007/978-3-319-28612-9_8. [Online]. Available: https://doi.org/10.1007/978-3-319-28612-9_8.

[12] E. Kaniusas, S. Kampusch, M. Tittgemeyer, *et al.*, "Current directions in the auricular vagus nerve stimulation I - a physiological perspective", en, *Front Neurosci*, vol. 13, p. 854, Aug. 2019.

[13] P. Schweitzer and L. E. Teichholz, "Carotid sinus massage. its diagnostic and therapeutic value in arrhythmias", en, *Am J Med*, vol. 78, no. 4, pp. 645–654, Apr. 1985.

[14] E. Ben-Menachem, "Vagus nerve stimulation, side effects, and long-term safety", en, *J Clin Neurophysiol*, vol. 18, no. 5, pp. 415–418, Sep. 2001.

[15] J. Liporace, D. Hucko, R. Morrow, *et al.*, "Vagal nerve stimulation: Adjustments to reduce painful side effects", *Neurology*, vol. 57, no. 5, pp. 885–886, 2001, ISSN: 0028-3878. DOI: 10.1212/WNL.57.5.885. eprint: https://n.neurology.org/content/57/5/885.full.pdf. [Online]. Available: https://n.neurology.org/content/57/5/885.

[16] A. Mertens, R. Raedt, S. Gadeyne, E. Carrette, P. Boon, and K. Vonck, "Recent advances in devices for vagus nerve stimulation", *Expert Review of Medical Devices*, vol. 15, no. 8, pp. 527–539, 2018, PMID: 30071175. DOI: 10.1080/17434440.2018.1507732. eprint: https://doi.org/10.1080/17434440.2018.1507732. [Online]. Available: https://doi.org/10.1080/17434440.2018.1507732.

[17] J. P. O'Reardon, P. Cristancho, and A. D. Peshek, "Vagus nerve stimulation (VNS) and treatment of depression: To the brainstem and beyond", en, *Psychiatry (Edgmont)*, vol. 3, no. 5, pp. 54–63, May 2006.

[18] C. B. Nemeroff, H. S. Mayberg, S. E. Krahl, *et al.*, "VNS therapy in treatment-resistant depression: Clinical evidence and putative neurobiological mechanisms", en, *Neuropsychopharmacology*, vol. 31, no. 7, pp. 1345–1355, Apr. 2006.

[19] J. Ellrich, "Transcutaneous vagus nerve stimulation", English, *European Neurological Review*, vol. 6, no. 4, pp. 254–256, 2011, ISSN: 1758-3837.

[20] K. J. Tracey, "The inflammatory reflex", en, *Nature*, vol. 420, no. 6917, pp. 853–859, 2002.

[21] C.-L. Cimpianu, W. Strube, P. Falkai, U. Palm, and A. Hasan, "Vagus nerve stimulation in psychiatry: A systematic review of the available evidence", *Journal of neural transmission (Vienna, Austria : 1996)*, vol. 124, no. 1, pp. 145–158, 2017, ISSN: 0300-9564. DOI: 10.1007/s00702-016-1642-2.

[22] V. Napadow, R. R. Edwards, C. M. Cahalan, *et al.*, "Evoked Pain Analgesia in Chronic Pelvic Pain Patients Using Respiratory-Gated Auricular Vagal Afferent Nerve Stimulation", *Pain Medicine*, vol. 13, no. 6, pp. 777–789, Jun. 2012, ISSN: 1526-2375. DOI: 10.1111/j.1526-4637.2012.01385.x. eprint: https://academic.oup.com/painmedicine/article-pdf/13/6/777/5207460/13-6-777.pdf. [Online]. Available: https://doi.org/10.1111/j.1526-4637.2012.01385.x.

[23] A. Straube, J. Ellrich, O. Eren, B. Blum, and R. Ruscheweyh, "Treatment of chronic migraine with transcutaneous stimulation of the auricular branch of the vagal nerve (auricular t-vns): A randomized, monocentric clinical trial", *The journal of headache and pain*, vol. 16, p. 543, 2015, ISSN: 1129-2369. DOI: 10.1186/s10194-015-0543-3. [Online]. Available: https://europepmc.org/articles/PMC4496420.

[24] S. Stavrakis, M. B. Humphrey, B. J. Scherlag, *et al.*, "Low-level transcutaneous electrical vagus nerve stimulation suppresses atrial fibrillation", *Journal of the American College of Cardiology*, vol. 65, no. 9, pp. 867–875, 2015.

[25] S. Stavrakis, J. A. Stoner, M. B. Humphrey, *et al.*, "Treat af (transcutaneous electrical vagus nerve stimulation to suppress atrial fibrillation) a randomized clinical trial", *Clinical Electrophysiology*, vol. 6, no. 3, pp. 282–291, 2020.

[26] J. Y. Y. Yap, C. Keatch, E. Lambert, W. Woods, P. R. Stoddart, and T. Kameneva, "Critical review of transcutaneous vagus nerve stimulation: Challenges for translation to clinical practice", *Frontiers in Neuroscience*, vol. 14, 2020, ISSN: 1662-453X. DOI: 10.3389/fnins.2020.00284. [Online]. Available: https://www.frontiersin.org/article/10.3389/fnins.2020.00284.

[27] E. T. Peuker and T. J. Filler, "The nerve supply of the human auricle", *Clinical Anatomy*, vol. 15, no. 1, pp. 35–37, 2002. DOI: https://doi.org/10.1002/ca.1089. eprint: https://onlinelibrary.wiley.com/doi/pdf/10.1002/ca.1089. [Online]. Available: https://onlinelibrary.wiley.com/doi/abs/10.1002/ca.1089.

[28] E. Frangos, J. Ellrich, and B. R. Komisaruk, "Non-invasive access to the vagus nerve central projections via electrical stimulation of the external ear: fMRI evidence in humans", en, *Brain Stimul*, vol. 8, no. 3, pp. 624–636, Dec. 2014.

[29] E. Kaniusas, S. Kampusch, M. Tittgemeyer, *et al.*, "Current directions in the auricular vagus nerve stimulation ii – an engineering perspective", *Frontiers in Neuroscience*, vol. 13, 2019, ISSN: 1662-453X. DOI: 10.3389/fnins.2019.00772. [Online]. Available: https://www.frontiersin.org/article/10.3389/fnins.2019.00772.

[30] L. Sörnmo and P. Laguna, "Chapter 1 - introduction", in *Bioelectrical Signal Processing in Cardiac and Neurological Applications*, ser. Biomedical Engineering, L. Sörnmo and P. Laguna, Eds., Burlington: Academic Press, 2005, pp. 1–24, ISBN: 978-0-12-437552-9. DOI: https://doi.org/10.1016/B978-012437552-9/50001-5. [Online]. Available: https://www.sciencedirect.com/science/article/pii/B9780124375529500015.

[31] V. Button, "Principles of measurement and transduction of biomedical variables", *Principles of Measurement and Transduction of Biomedical Variables*, pp. 1–370, Jan. 2015.

[32] L. Sörnmo and P. Laguna, "Chapter 6 - the electrocardiogram—a brief background", in *Bioelectrical Signal Processing in Cardiac and Neurological Applications*, ser. Biomedical Engineering, L. Sörnmo and P. Laguna, Eds., Burlington: Academic Press, 2005, pp. 411–452, ISBN: 978-0-12-437552-9. DOI: https://doi.org/10.1016/B978-012437552-9/50006-4. [Online]. Available: https://www.sciencedirect.com/science/article/pii/B9780124375529500064.

[33] A. Işın and S. Özdalili, "Cardiac arrhythmia detection using deep learning", *Procedia Computer Science*, vol. 120, pp. 268–275, Jan. 2017. DOI: 10.1016/j.procs.2017.11.238.

[34] F. Shaffer and J. P. Ginsberg, "An overview of heart rate variability metrics and norms", *Frontiers in Public Health*, vol. 5, 2017, ISSN: 2296-2565. DOI: 10.3389/fpubh.2017.00258. [Online]. Available: https://www.frontiersin.org/articles/10.3389/fpubh.2017.00258.

[35] N. Sviridova and K. Sakai, "Human photoplethysmogram: New insight into chaotic characteristics", *Chaos, Solitons & Fractals*, vol. 77, pp. 53–63, 2015, ISSN: 0960-0779. DOI: https://doi.org/10.1016/j.chaos.2015.05.005. [Online]. Available: https://www.sciencedirect.com/science/article/pii/S0960077915001344.

[36] B. Dabiri, K. Zeiner, A. Nativel, and E. Kaniusas, "Multifunctional auricular vagus nerve stimulator for closed-loop application", in *2021 34th SBC/SBMicro/IEEE/ACM Symposium on Integrated Circuits and Systems Design (SBCCI)*, 2021, pp. 1–5. DOI: 10.1109/SBCCI53441.2021.9529999.

[37] Maxim Integrated Products, Inc. "Max86150 integrated photoplethysmogram and electrocardiogram bio-sensor module for mobile health". (2018), [Online]. Available: https://datasheets.maximintegrated.com/en/ds/MAX86150.pdf (visited on 07/11/2022).

[38] Maxim Integrated Products, Inc. "App note6843: How to configure the optimal settings for the best ppg and ecg performance in the max86150". (2014), [Online]. Available: https://pdfserv.maximintegrated.com/en/an/an6843-settings-for-PPG-ECG-MAX86150.pdf (visited on 04/26/2022).

[39] D. W. Boyd, "Chapter 8 - stochastic analysis", in *Systems Analysis and Modeling*, D. W. Boyd, Ed., San Diego: Academic Press, 2001, pp. 211–227, ISBN: 978-0-12-121851-5. DOI: https://doi.org/10.1016/B978-012121851-5/50008-3.